JOURNAL OF QUATERNARY SCIENCE (2021) 1–17 ISSN 0267-8179. DOI: 10.1002/jqs.3320

JQS Journal of Quaternary Science QRA Quaternary Research Association

Larger floods of Himalayan foothill rivers sustained flows in the Ghaggar–Hakra channel during Harappan age

AJIT SINGH,[1]* VIKRANT JAIN,[1] MICHEL DANINO,[2] NAVEEN CHAUHAN,[3] RAHUL KUMAR KAUSHAL,[1,3] SHANTAMOY GUHA[1] and V. N. PRABHAKAR[2]

[1]Discipline of Earth Sciences, IIT Gandhinagar, Gandhinagar, India
[2]Archaeological Sciences Centre, IIT Gandhinagar, Gandhinagar, India
[3]Atomic, Molecular and Optical Physics Division, PRL Ahmedabad, India

Received 12 August 2020; Revised 14 April 2021; Accepted 20 April 2021

ABSTRACT: The human–landform interaction in the region of the Ghaggar–Hakra palaeochannel in the northwest Indo-Gangetic plains during the Bronze Age Indus/Harappan civilisation (~4.6–3.9 thousand years before the present, ka BP) remains an enigmatic case due to a paucity of evidence regarding the hydrology of the then existing river. Here, we estimated the palaeohydrology of the foothill Markanda River in the sub-Himalayan catchment of the Ghaggar–Hakra (G–H) palaeochannel. Our morphology and chronology results show aggradation of a fan (57.7 ka) during the Late Pleistocene and T–1 to T–5 fluvial terraces (13.1 to 6.0 ka) during the terminal Pleistocene to Holocene, and deposition of palaeoflood sediments (3.9–3.8 ka) over the T–3 terraces during the Late Holocene. Considering the known uplift rates along the Himalayan frontal thrust, and our estimated aggradation rates, we derived channel palaeogeometry and calculated peak discharge at the site of palaeoflood deposits. We conclude that the Markanda River's peak discharge was several orders of magnitude higher during the Late Holocene than the modern-day peak discharge of 100-year return period. The palaeoflood deposits represent larger flooding of the foothill rivers that sustained flows in the downstream reaches of the Ghaggar–Hakra palaeochannel during the Late Harappan civilisation. Copyright © 2021 John Wiley & Sons, Ltd.

KEYWORDS: Ghaggar–Hakra; Harappa; Indus civilization; Markanda valley; palaeoflood; Sarasvati

Introduction

The conjectured past existence of the Sarasvati river between the drainage divide of the rivers Sutlej in the west and Yamuna in the east in the northwest Indo-Gangetic plains has been a major focus of research. As early as in 1788, Surveyor General James Rennel marked the monsoon-fed Ghaggar (Fig. 1) as "Sursooty" in his *Memoir of a Map of Hindoostan* (1788). Lieutenant Colonel James Tod in his *Annals and Antiquities of Rajasthan* (1832) mapped ruins of large towns where the Ghaggar River dried up in the Thar Desert. Major Colvin (1833) and Major F. Mackeson (1844) in their ground surveys (referenced in Danino, 2010) reported sweet-water wells inside and brackish-water wells outside the Ghaggar channel. Following these, the French geographer L. Vivien de Saint-Martin (1860) suggested that the dry river bed occupied by the Ghaggar River must be the relic of the Sarasvati River described in the Vedic hymns. The *Nadistuti Sukta* ("hymn in praise of rivers") of Rigveda (75.5 & 6) mentions the geographical position of the River Sarasvati between the Yamuna and the Sutlej. There followed detailed discussions by geologists, geographers and Sanskritists (e.g. Oldham, 1874, 1886; Stein, 1917; Wilhelmy 1969). With Luigi Pio Tessitori in the 1910s and Aurel Stein in the 1940s (Stein, 1942), archaeological explorations began in the river basin, followed by several surveys after the Partition of India in 1947 (Danino, 2010). The presence of Mature Harappan settlements (4.6–3.9 ka BP), including a few major ones like Banawali, Kalibangan, Rakhigarhi and Kunal, along the Ghaggar–Hakra (G–H) palaeochannel led scholars to believe that it was possibly occupied by a large river system, which they identified with the Sarasvati of Vedic literature (Joshi *et al.*, 1984; Lal, 1997; Kenoyer, 1998; Possehl, 1999; Misra, 2001; Valdiya, 2002, 2017).

Currently, the drainage divide is occupied by Himalayan foothill rivers such as Patiala Rao, Ghaggar, Markanda, Dangri and Chautang (Fig. 1). Using satellite images, three major palaeochannels were identified in the drainage divide (Pal *et al.*, 1980). The most prominent ones are the palaeo-Sutlej and the G–H palaeochannel; the former is traceable up to the Sutlej River exit upstream and joins the latter that roughly follows the modern Ghaggar River (Fig. 1). Besides the palaeo-Sutlej, two different flow paths of the palaeo-Yamuna connect with the G–H palaeochannel (Fig. 1). Channel Y2, which corresponds to the modern Chautang River, runs southwest to join the Ghaggar River, while channel Y1 is located along the modern Markanda River.

In the last two decades, research has been focused on the G–H palaeochannel (Saini *et al.*, 2009; Clift *et al.*, 2012; Giosan *et al.*, 2012; Singh *et al.*, 2017; Durcan et al., 2019; Chatterjee *et al.*, 2019) and to some extent on channel Y2 (palaeo-Yamuna) (Dave *et al.*, 2019; Khan and Sinha, 2019). However, these chrono-stratigraphic records are insufficient to estimate the evolution of the G–H palaeochannel's hydrological regime, in particular during the Holocene when the palaeochannel was deteriorating to an ephemeral river after the avulsion of the source rivers, the Sutlej and the Yamuna (Clift *et al.*, 2012, Singh and Sinha, 2019). Though drying up of these palaeochannels due to the weakening of monsoonal precipitation in the Holocene has been proposed (Singh *et al.*, 1972; Wasson *et al.*, 1984; Staubwasser *et al.*, 2003; Berkelhammer *et al.*, 2012; Dixit *et al.*, 2014b), any direct evidence/estimate of palaeohydrology of the G–H

*Correspondence: A. Singh, as above.
E-mail: ajit268@gmail.com; ajit.singh@iitgn.ac.in

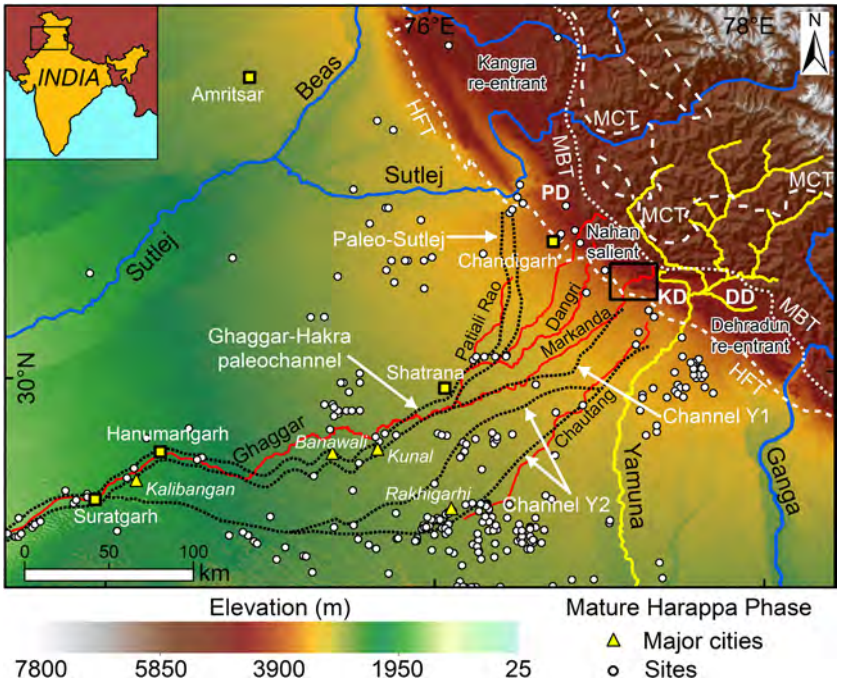

Figure 1. Digital elevation model based topographic map of north-western Himalaya. Also shown are modern Himalayan and foothill rivers along with the network of Ghaggar-Hakra paleochannels (Pal et al., 1980). Earlier studies mainly focused on the paleo-Sutlej channel and channel Y2. Present study focused on the Markanda valley (black lined rectangle) in the catchment of the channel Y1. Major tectonic structures are MCT-Main central thrust, MBT-Main boundary thrust, HFT-Himalayan frontal thrust. Major intermontane valleys are PD- Pinjaur dun, KD-Kiarda dun, and DD- Dehradun. [Color figure can be viewed at wileyonlinelibrary.com]

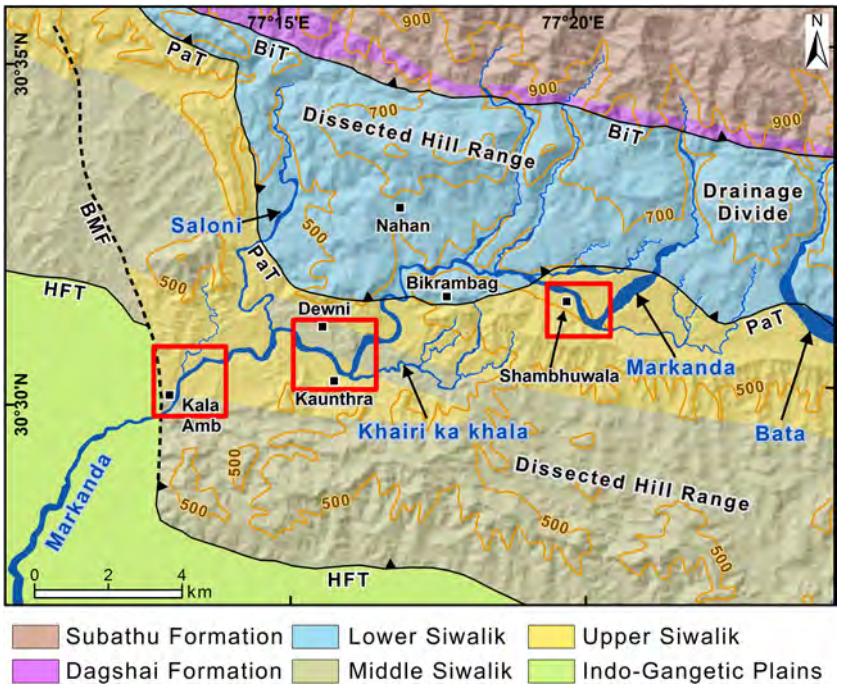

Figure 2. Litho-tectonic map of the Markanda valley and nearby area. Major lithology includes pre-tertiary rocks of the Subathu and Dagshai formations in the north followed by the sandstone, mudstone, and conglomerate rocks of Siwalik group. Major tectonic structures include BiT- Bilaspur thrust, PaT- Paonta thrust, HFT-Himalayan frontal thrust, and strike slip fault BMF-Black mango fault. Three red rectangles mark the three study windows near Shambhuwala, Kaunthra and Kala Amb. Contours (500, 700, 900) show elevation in masl. [Color figure can be viewed at wileyonlinelibrary.com]

paleochannel using fluvial archives has never been attempted. Knowledge of the palaeohydrology of the G–H palaeochannel is also required to test the hypothesis that the Himalayan foothill rivers during Harappan times had sufficient water flows to sustain the civilisation even in the absence of a large perennial Himalayan-sourced river.

In this work, we reconstruct the evolutionary history of the Markanda valley in the sub-Himalayan catchment of the Ghaggar–Hakra palaeochannel. We simulated model-based modern discharge, in calibration with the observed discharge, to estimate peak discharge during high-magnitude flood events of the 100-year return period. We identified palaeoflood deposits to estimate the palaeohydrology of the Markanda River. Depositional chronology of the palaeoflood deposits was used to establish the timing of hydrological changes in the Markanda valley and to compare such changes across the northwestern Himalayan foothill rivers. Finally, we explore the implications of hydrological changes of the foothill rivers on the G–H palaeochannel and Harappan settlements.

Methods and approach

In the present study, we mapped the morphology, characterised sedimentology and estimated depositional chronology of fluvial terraces in the Markanda valley to estimate changes in hydrology (flood discharge) of the Markanda River during the Holocene. Digital elevation models (DEM), topographic sheets and satellite imagery were used to map geomorphic units. High-resolution mapping of the fluvial terraces and river cross-sections was done using real-time kinematics DGPS (RTKDGPS) in the field. Luminescence dating was used to estimate the depositional ages of fluvial terrace fill sediments. Together with valley cross-sections, the depositional ages were

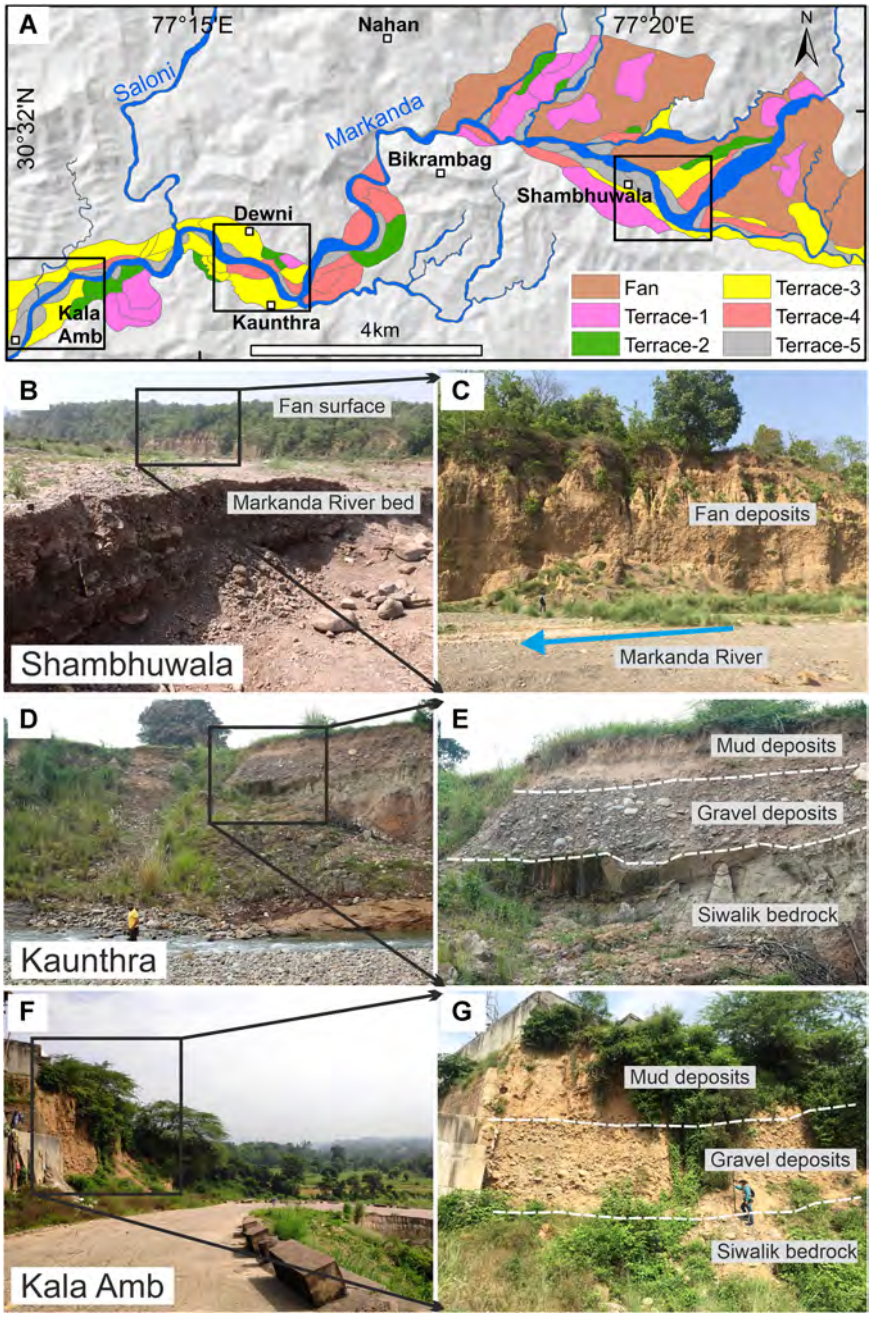

Figure 3. (A) Geomorphic map of the Markanda valley with boxes showing study windows. SRTM based shaded relief map used in the background. Major geomorphic units in the upper Markanda valley (UMV), upstream of Bikrambag, includes extensive fan surfaces with higher elevation fluvial strath terraces (T–1 and T–2). Lower Markanda valley (LMV) is composed of lower elevation fluvial strath terraces (T–3 to T–5). (B) fan surface and (C) fan section exposed in a cliff near Shambhuwala. (D) and (E) Strath fluvial terrace showing Siwalik bedrock overlain by gravel and mud layer deposits exposed in a cliff near Kaunthra. (F) and (G) Strath fluvial terrace showing Siwalik bedrock overlain by gravel and mud layer deposits exposed in a cliff near Kala Amb. [Color figure can be viewed at wileyonlinelibrary.com]

Table 1. Regional litho-tectonic setting of the Markanda valley (after Raiverman et al., 1983)

	Rock unit	Lithology	Age
Pre-Tertiary		Clastic and carbonates (Krol limestone)	Proterozoic
		Main boundary thrust	
	Kasauli	Micaceous sandstone	Miocene
Lower Tertiary	Dagshai	Red/green sandstone and mudstones	Oligocene
	Subathu	Shales with limestone bands	Palaeocene–Eocene
		Main boundary fault	
	Lower Siwaliks	Mudstones and sandstones	
		Nahan thrust	
	Upper	Sandstone and conglomerate	Middle Pleistocene
Siwalik group	Middle	Sandstone and subordinate mudstone	Late Miocene
	Lower	Mudstones and sandstones	Mid-Miocene
		Himalayan frontal thrust	
		Indo-Gangetic alluvial plains	

Table 2. Summary of radionuclide concentration, cosmic radiation-based dose rates, moisture content, equivalent dose (D_e), total dose rate (D_r), and luminescence age of the analysed sediment samples

Sample	U (ppm)	Th (ppm)	K (%)	CR (Gy/ka)	Water (%)	D_e (Gy)	Over dispersion (%)	Aliquots accepted (measured)	D_r (Gy/ka)	Age (ka)
mkd-1*	2.36 ± 0.08	9.50 ± 0.39	1.33 ± 0.04	0.173 ± 0.005	15.2	14.2 ± 0.1	40.0	24 (24)	2.96 ± 0.17	6.0 ± 0.3
mkd-2**	2.55 ± 0.08	10.75 ± 0.40	1.75 ± 0.04	0.160 ± 0.006	17.0	13.0 ± 0.1	33.9	20 (24)	3.38 ± 0.17	8.8 ± 0.8
mkd-3†	3.27 ± 0.08	15.39 ± 0.48	2.25 ± 0.05	0.056 ± 0.004	22.2	221.4 ± 0.1	44.3	13 (17)	3.84 ± 0.13	57.7 ± 1.9
mkd-4*	2.33 ± 0.08	8.88 ± 0.37	1.21 ± 0.04	0.146 ± 0.006	18.6	16.6 ± 0.1	46.4	21 (24)	2.72 ± 0.17	7.8 ± 0.5
mkd-5**	3.66 ± 0.10	8.70 ± 0.36	1.14 ± 0.04	0.128 ± 0.005	15.5	19.9 ± 0.1	33.8	22 (24)	2.95 ± 0.17	13.1 ± 1.2
mkd-6*	1.91 ± 0.07	9.09 ± 0.38	0.70 ± 0.03	0.150 ± 0.006	18.0	6.6 ± 0.1	50.9	23 (24)	2.23 ± 0.16	3.8 ± 0.3
mkd-7*	3.10 ± 0.09	11.39 ± 0.43	1.01 ± 0.03	0.159 ± 0.005	16.1	14.2 ± 0.1	32.3	19 (24)	2.90 ± 0.17	10.9 ± 1.0
mkd-8**	3.59 ± 0.10	14.81 ± 0.55	2.04 ± 0.05	0.120 ± 0.006	27.5	15.8 ± 0.7	15.4	23 (24)	3.72 ± 0.19	3.9 ± 0.2
mkd-9*	2.23 ± 0.07	11.54 ± 0.44	0.92 ± 0.03	0.126 ± 0.005	14.9	6.3 ± 0.1	51.8	21 (24)	2.65 ± 0.16	6.1 ± 0.4
mkd-10**	2.50 ± 0.08	10.24 ± 0.42	1.17 ± 0.04	0.153 ± 0.006	19.2	18.9 ± 0.1	30.5	23 (24)	2.79 ± 0.17	13.1 ± 1.2

*D_e estimated using minimum age model (MAM-3); **D_e estimated using central age model (CAM); †K-feldspar-based age (MAM-3).

used to identify the palaeogeometry of the Markanda River. Palaeoflood discharge was estimated by using palaeogeometrical dimensions in empirical equations that relate bankfull discharge to channel hydraulic geometry. Modern discharge of the Markanda River is available for a very limited time interval (1976–1978) of strong monsoon years (Parthasarathy *et al.*, 1994), and was extended through the soil and water analysis tool (SWAT).

Morphology and sedimentology

The DEM used for the detailed geomorphic map (Fig. 3A) is the NASA Shuttle Radar Topography Mission (SRTM) DEM with 30 m spatial resolution (Farr *et al.*, 2007). Satellite data consisted of LANDSAT 7 (30 m resolution) imagery using spectral bands 456 (near-infrared, short-wave infrared and thermal infrared) to enhance the spectral and spatial properties. Survey of India topographical maps (scale 1:50 000) were also used for mapping and to identify town and village locations. The detailed topographical survey for valley cross-section and channel geometry such as channel width and depth, dimensions and elevation of fluvial terraces was done using a real-time kinematic (RTKDGPS) survey.

Sedimentology of fluvial deposits was recorded through observation of sedimentary characteristics exposed at cliff sections and cuttings along the Markanda River. Observed sedimentary characteristics are colour, grain size, sorting, texture, fabric, lithology, stratification and bedding geometry. Sediment logs were prepared and different lithofacies were identified and grouped into fluvial gravel/sand, fan silt–mud, palaeoflood and alluvial fan debris. Together, the geomorphic, topographic and sedimentary information was used to prepare channel cross-sections along three study windows (Shambhuwala, Kaunthra and Kala Amb) to focus on the palaeohydrological analysis (Figs. 3A and S1).

Optically stimulated luminescence dating

Optically stimulated luminescence (OSL) dating was used to establish the chronology of the fluvial terrace levels. OSL dating estimates the time of last light exposure, i.e. the burial of sediment approximately coinciding with the depositional event. Sediment samples were collected at different levels of the fluvial landforms (fan and terraces) along the longitudinal profile of the Markanda valley (Table 2). OSL dating was done at the Physical Research Laboratory, Ahmedabad, India. Details of sample processing for extraction of quartz grains and analytical protocol are given in the supplementary material. Fig. 4A shows the OSL and infrared stimulated luminescence (IRSL) (inset) response for one of the quartz samples. The samples had a low IRSL response, indicating that the extracted quartz is pure which is further used for estimating the palaeodoses.

Equivalent dose (D_e) is estimated from the OSL of quartz extracts using standard single aliquot regeneration (Murray and Wintle, 2000) measurements (Fig. 4B). The estimated doses had significant scatter (overdispersion (OD) ~30.5 to 51.8%; Table 2) as shown in Figs. 4C and S2. The statistical analysis was performed on dose distribution considering several suggested models (Arnold *et al.*, 2007; Chauhan and

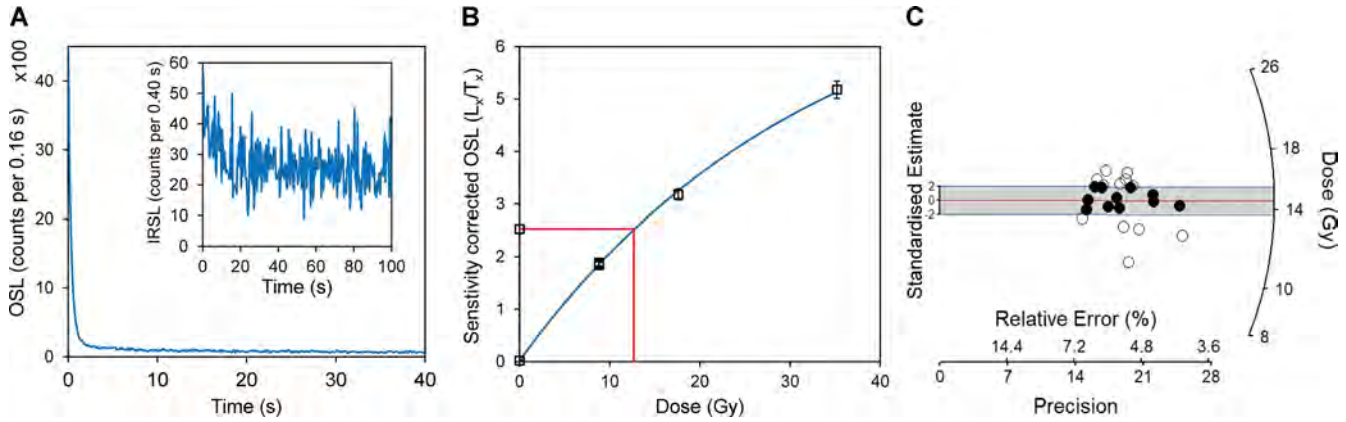

Figure 4. Measurement results for one of the samples (mkd-8). (A) OSL decay curve and IRSL test result of quartz samples (inset). (B) Growth curve fitted using an exponential function for quartz along with the natural signal (marked in red). (C) Radial plot of individual De of the sample. Grey shaded area represents ±2σ. [Color figure can be viewed at wileyonlinelibrary.com]

Singhvi, 2011; Chauhan and Morthekai, 2017) and used to decide the appropriate age model viz. the central age model (CAM) or the minimum age model for calculation of D_e (Table 2). For all 10 samples, the models agreed on use of mean (CAM) or minimum age models.

For the environmental dose rate, the elemental concentrations of U, Th and K were measured using gamma-ray spectrometry in an ultra-low background Ortec high purity germanium (HPGe) detector. The dose rates and ages (Table 2) are estimated using standard software (DRc: DR calculator) which uses an infinite matrix assumption and takes into consideration the effect of water, beta attenuation, internal dose rate, cosmic ray dose rate contribution and grain size (Tsakalos *et al.*, 2016).

Modern discharge estimates

Despite our repeated efforts, longer duration data for modern-day observed discharge at river gauge stations remained unavailable except for the observed monthly discharge data available for 1976–1978 (Parkash *et al.*, 1983). Therefore, the modern discharge of the Markanda River at Kala Amb (Fig. 1), was estimated using a physically based, semi-distributed and continuous-time hydrological model called SWAT. The SWAT model, developed by the U.S. Department of Agriculture–Agriculture Research Service, simulates hydrological processes on the basis of physical parameters at a basin-scale (Arnold *et al.*, 1998). Hydrological process simulation is based on the water balance equation:

$$SW_t = SW_0 + \sum_{i=1}^{t}\left(R_{day} - Q_{surf} - E_a - w_{seep} - Q_{gw}\right) \quad (1)$$

In Equation 1, SW_t is final soil water content (mm); SW_0 is initial soil water content on day i (mm); t is time (day); R_{day} is amount of precipitation on day i (mm); Q_{surf} is amount of surface runoff on day i (mm); E_a is amount of evapotranspiration on day i (mm); w_{seep} is amount of water entering the vadose zone from the soil profile on day i (mm); Q_{gw} is amount of return flow on day i (mm). We simulated discharge values for the period of 38 years (1970–2007) using the SWAT model by following the procedures given in Kaushal *et al.* (2020). Details on data calibration and model protocols are given in the supplementary material.

The SWAT-based daily peak discharge (1970–2007) was used to estimate the return period (Tr) for flood discharge (extreme event). This was done using the log-Pearson type III distribution which is a statistical technique for fitting frequency distribution data to predict flood discharge for a range of return periods. Unlike normal distribution that accounts for standard deviation and mean only, the log-Pearson distribution considers skewness. The smaller the skewness, the log-Pearson distribution approximates a normal distribution. The advantage of this technique is that extrapolation of discharge values can be made for events with return periods beyond the observed flood events. The probabilities of floods (1/Tr) of various sizes can be extracted from the frequency distribution curve. Equation 2 is used to estimate the discharge of a given return period (Q_T), where Q is discharge in each of the years; K is the frequency factor; Cs is skewness coefficient. The skewness coefficient (Cs), calculated using Equation 3, is the estimate for the station of interest. The respective values of frequency factor (K) for a given value of skewness coefficient (Cs) and return period (Tr) of interest (Haan, 1977) is used in Equation 2 to compute Q_T. Peak discharge values were estimated for return periods of 2, 5, 10, 25, 50 and 100 years.

$$\log Q_T = \text{average } \log Q + K_{(Tr,Cs)}\sigma_{\log Q} \quad (2)$$

$$Cs = \frac{n^*\sum((\log Q - \overline{logQ})^3)}{(n-1)(n-2)(\sigma_{logQ})^3} \quad (3)$$

Palaeodischarge estimate

Palaeohydrological studies use erosional and depositional features as an indicator of past river stage to estimate palaeodischarge or more specifically peak discharge during past flooding event(s) (Baker, 1973, 1987). Palaeoflood or slack water deposits are depositional features that accumulate from suspension during major flood events in protected areas of reduced velocity such as tributary confluences (Baker *et al.*, 1983; O'Connor, 1993; Kale *et al.*, 2000; Baker, 2008; Srivastava *et al.*, 2017). In the present study, palaeoflood discharge is estimated using Equation 4, where Q = discharge, (m^3/s), v = velocity (m/s), A = flow cross-section area (m^2).

$$Q = vA \quad (4)$$

The velocity, v, was obtained by a flow resistance formula. We adopted the widely used Manning's equation (Equation 5),

$$v = \left(\frac{1}{n}\right)R^{2/3}S^{1/2} \quad (5)$$

where R is the hydraulic radius, (m); S is channel slope, (m/m); n = Manning's roughness coefficient, which represents the physical characteristics of the channel bed.

A tool, called ChanGe tool, was designed in the MATLAB program that uses channel cross-section to compute wetted perimeter, hydraulic radius, average depth and cross-section area for the channel up to the elevation of a palaeoflood deposit (Guha *et al.*, 2020). Details on the workflow and algorithm of the ChanGe tool are given in the supplementary material. Additionally, we also used constitutive flow resistance equations to calculate palaeodischarge (Table S1). These are modified equations on the basis of calibration and validation using a discharge database of 103 natural rivers (Bjerklie *et al.*, 2005).

Results

Fan surfaces and fluvial terraces

An extensive alluvial fan surface and five levels of fluvial terraces were identified as geomorphic units in the Markanda valley (Fig. 3A). On the basis of the distribution of these units, the valley is divided into two parts. The west-flowing upper Markanda valley (UMV) upstream of Bikrambag is mostly occupied by fan deposits, whereas the south-flowing lower Markanda valley (LMV) downstream mainly consists of fluvial terraces. In addition, there are hills with an elevation range of 500 to 900 m. These dissected hills are composed of Siwalik rocks. The major river is the southwest-flowing Markanda separated from the southeast-flowing Bata River by a drainage divide. The major tributaries of the Markanda River are Khairi ka Khala with confluence upstream of Kaunthra village, Saloni River (at elevation ~373 m) with confluence near Dewni village, and a much smaller tributary near Kala Amb (Fig. 3A).

The UMV is structurally bounded between dissected hill ranges and the Bilaspur thrust in the north, and the Paonta thrust in the south (Fig. 2). The fan surface has an average elevation of 800 m in the proximal and ~450 m in the distal part. The proximal fan unit consists of massive, clast- to matrix-supported angular pebble conglomerates with some interbedded sand layers (Fig. 3B). Fan surfaces are incised by south-flowing antecedent drainage consisting of the Markanda

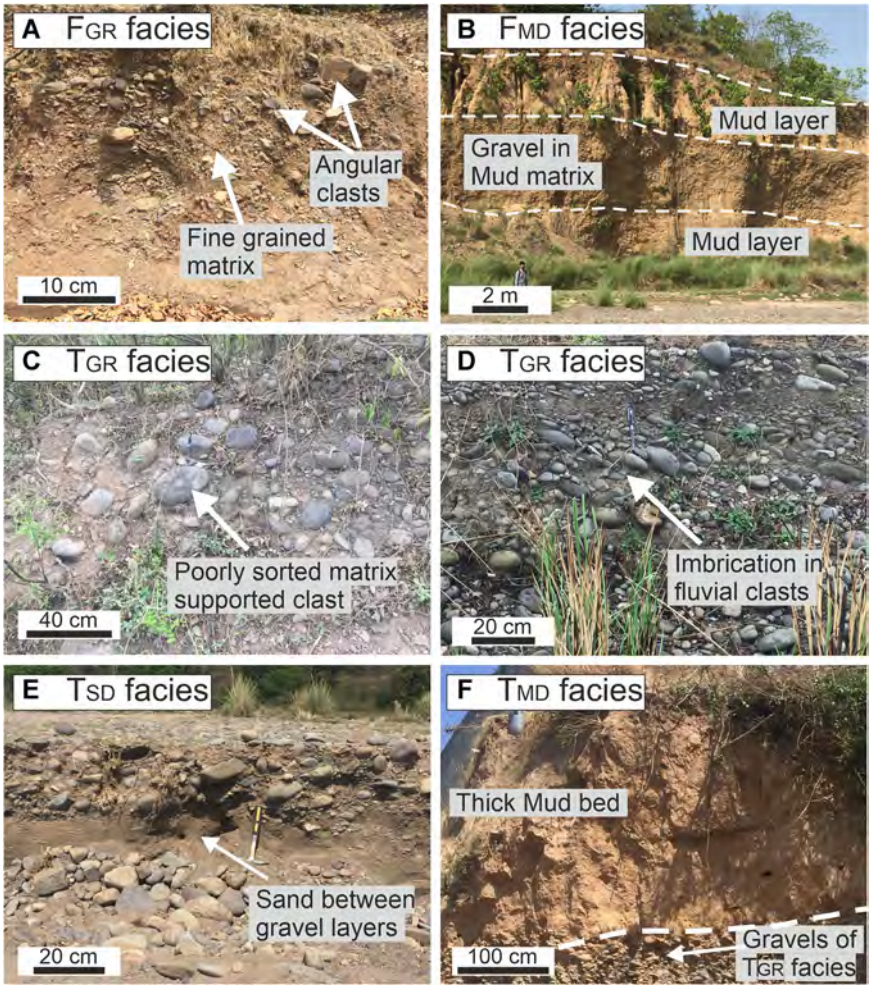

Figure 5. Field photographs of major sediment facies as observed in exposed cliff sections of geomorphic units. (A) proximal fan facies composed of matrix to clast supported, disorganized angular pebbles to boulders. (B) distal fan facies composed of stratified layers of yellow mud. (C) and (D) matrix supported gravel deposits in fluvial terraces. (E) sand layers between the gravelly deposits of fluvial terraces. (F) massive and unstratified deposits of yellow mud/silt overlying gravelly deposits of fluvial terraces. [Color figure can be viewed at wileyonlinelibrary.com]

Table 3. Systematic description of the sedimentary facies in the Markanda valley

Facies	Description	Depositional environment
Fan deposits		
F_{GR}: Fan gravels	Matrix- to clast-supported, disorganised, angular and unsorted clasts. Clast size (30–5 cm) range from pebble to boulder. Clast lithology quartzite and sandstone.	Aggradation of debris flow sediments in proximal fan environment.
F_{MD}: Stratified mud	Fine to very fine yellow massive mud, stratified layers, occasionally contains pebbly layers.	Stacked fluvial sediments in a distal fan environment.
Terrace deposits		
T_{GR}: Fluvial gravels	Rounded to sub-rounded, poorly sorted boulder to pebble-size clast in sandy matrix. Clasts occasionally show imbrication. Clast composition is dominated by sandstone and quartzite.	Clast- and matrix-supported cobble gravel bedload of fluvial origin deposited in channel bedload and on longitudinal bars.
T_{SD}: Fine sand	Fine to coarse-grained, grey, cross-stratified to parallel lamination. Stream flow deposits.	Sand lenses interbedded in the clastic deposits of fluvial origin.
T_{MD}: Yellow mud	Silt/mud sediment overlying the clastic deposits of older terraces. Massive deposits, no stratification/pedogenesis.	Fine-grained silt and sand fall rapidly out of suspension during large floods.

River and its tributaries, which are embanked by fluvial terraces. The distal fan deposits are exposed along the west-flowing reach of the main Markanda River towards Bikrambag. These nearly planar fan deposits are mainly composed of finer sediments interlayered with gravel material. Five levels of terraces were labelled as T–1 (highest elevation) to T–5 (lowest elevation) (Fig. 3B–C). Fluvial terraces, T–1 and T–2, are present along the Markanda River and its north-to-south-flowing tributaries (in the UMV), whereas terraces T–3 and T–5 are present on the westward-flowing Markanda River (in the LMV) (Fig. 3D–E). Deposits of the terraces T–1 and T–2 overlie the incised fan surface, thus forming the typical cut and fill terraces (Dutta *et al.*, 2012).

In the LMV, five levels of rock-cut or strath terraces are present, in which gravelly deposits of the terraces are underlain by the former valley floor of Siwalik bedrock (Fig. 3F–G). These terraces are at an elevation of >25 m for T–1, 25–16 m for T–2, 15–11 m for T–3, 10–6 m for T–4, and <5 m for T–5 as measured above the bed level of the Markanda River. Lateral extent or width of the terraces varies from 0.5 to 2 km, suggesting quite a wide valley of the Markanda River in the past. Of all the terraces, T–3 is the most developed and spatially extensive, and is observed at the Bikrambag, Kaunthra, Dewni and Kala Amb areas. The terraces are of non-paired type, developed over alternating

beds of claystone and sandstone, and of boulder conglomerates of Upper Siwalik age. The sediment capping over the strath terraces ranges from about 2 to 5 m in thickness, composed of pebbles and gravel, and at a few locations is overlain by light grey fine sand or sandy mud/silt.

Sedimentology and palaeoflood deposits

Five distinct sediment facies are identified for the late Quaternary sediments in the Markanda valley (Fig. 5). These are categorised into fan deposits and terrace deposits, on the basis of their occurrence in the geomorphic units (Table 3). The F_{GR} facies, at the proximal part of the fan, consists of angular clasts (mostly 2–10 cm and up to 20 cm in size) embedded in a fine-grained matrix. The sedimentary texture is occasionally clast-supported to dominantly matrix-supported disorganised pebbles and boulders (Fig. 5A). Clast includes quartzite, sandstone of different colours (and composition), and less abundant smaller clasts of shale, phyllite and schist. The matrix is composed of yellow silt to mud-sized grains. This suggests deposition by cohesive clast-rich and hyperconcentrated debris flow. The F_{MD} facies, at the distal margin of the fan, consists of deposits of yellow mud. These stratified deposits form ~0.5 to 1 m thick mud layers with interlayers of clast-in-mud deposits (Fig. 5B). The clasts are smaller (2–6 cm) than the clasts of the F_{GR} facies. This is interpreted to represent sediment saturated flows; however, the presence of clastic inter-layers suggest intervals of bedload transport of gravels.

The T_{GR} facies, extensively present in fluvial terraces T–1 to T–5, consists of sub-rounded to rounded clasts embedded in a fine sand matrix. The sedimentary texture is clast-supported to dominantly matrix-supported. Clast is dominantly sandstone of a different colour (and composition) in the matrix in fine to medium-grained sand. It is interpreted to represent channel aggradation periods in the Markanda valley (Fig. 5C–D). The T_{SD} facies, overlying deposits of T_{GR} facies in the T–3 terrace, composed of fine-grained grey sand (Fig. 5E). In a 13.5 m high cliff section near Bikrambag village (Fig. 3A), sand forms a 1.2 m thick layer overlain by a thin layer of soil (Fig. 3E). The T_{MD} facies are composed of yellow mud and overlies deposits of T_{GR} facies. The 4 m thick layer of T_{MD} facies is overlying 8 m thick gravel deposits (T_{GR}) of T–3 terrace (Fig. 3E). The mud layer in a cliff section was observed at 30 m above the channel bed (Fig. 3F–G). These facies (T_{SD} and T_{MD}) are interpreted as palaeoflood deposits on the basis of (a) their spatial occurrence near tributary confluences of the Markanda River, (b) forming stratigraphically distinct layers above typical gravel deposits of the T–3 terrace, and (c) as discussed later, their young age that are chronologically distinct from the underlying older deposits.

The palaeoflood deposits are observed at two locations: at Kaunthra near the confluence of the Khairi ka Khala tributary, and at Kala Amb near the confluence of the Dankawala tributary of the Markanda River (Fig. 2). The topographical survey shows that these 1.2 m and 4 m thick deposits are ~ 13.5 and 30 m above the present channel bed, respectively, at Kaunthra and Kala Amb. As only large floods could have reached such high stages, these deposits were used for palaeohydrological analyses.

Chronology of fan and terraces

The distribution of luminescence ages of sediments collected from fluvial terraces and channel bed ranges between 13.1 ± 1.2 and 6.0 ± 0.3 ka (Table 2). While the only sample (mkd–3) collected at a cliff section on the distal fan yields an age of 57.7 ± 1.9 ka indicating fan development in the Markanda valley during the Pleistocene (Fig. 6). At Shambhuwala, sample mkd–2 collected in the sand lens of gravel deposits in the T–5 terrace yields an age of 8.8 ± 0.8 ka (Fig. 6B). Downstream of this, at the Kaunthra section, sample mkd–1 collected in the fine sand lens of gravel bar deposit yields an age of 6.0 ± 0.3 ka, sample mkd–7 collected in the sand lens of gravel deposits in the T–4 terrace yields an age of 10.9 ± 1.0 ka, and sample mkd–5 collected in the sand lens of gravel deposits in the T–3 terrace yields an age of 13.1 ± 1.2 ka (Fig. 6C). Further downstream at the Kala Amb section, sample mkd–9 collected in the sand lens of gravel deposits in the T–4 terrace yields an age of 6.1 ± 0.4 ka and the sample mkd–10 collected in sand deposits in the T–5 terrace yields an age of 13.1 ± 1.2 ka (Fig. 6D). At Kaunthra, sample mkd–6 collected in palaeoflood sediments composed of fine sand, overlying gravel deposits of the T–3 terrace, yields an age of 3.8 ± 0.3 ka. Downstream, at Kala Amb, sample mkd–8 collected in palaeoflood sediments composed of silt to fine sand, overlying gravel deposits of the T–3 terrace yields an age of 3.9 ± 0.2 ka.

Estimates of river hydrology

The observed data (after Parkash *et al.*, 1983) for the Markanda River ranges from a minimum of 0.5×10^6 m^3/month (average monthly discharge 0.2 m^3/s) during pre-monsoon (May) to a maximum of 58.2×10^6 m^3/month (average monthly discharge 22 m^3/s) during the monsoon (August) period. Our SWAT model-based estimates of average monthly discharge values (Fig. 7A) show good accuracy with the observed dataset (R^2 = 0.9 and Nash–Sutcliffe = 0.89) and was able to capture the temporal variability (Fig. 7A inset). Further, SWAT-derived mean monthly discharge data were compared with mean monthly precipitation for the duration of 38 years, which highlights good correlation (R^2 = 0.96) (Fig. 7B–C). Therefore, we applied log-Pearson type III analysis to our modelled peak (daily) discharge data for duration 1970 to 2007 to estimate flood discharge for a 100-year return period (≈300 m^3/s) which is nearly 13 times the modern average monthly discharge (22 m^3/s) (Fig. 7D).

Flood discharge estimates using palaeoflood deposits require estimates of dimensions of palaeochannel geometry (Bauer and Klinger, 2010). Therefore, we attempted to estimate the discharge values by modifying the bed level of present channel geometry using palaeoriver surfaces (river terraces). The depth of the palaeochannel geometry was estimated from fluvial aggradation records, reconstructed using OSL dating of fluvial terraces in the present study, and tectonically controlled fluvial incision near Kala Amb (Kumar *et al.*, 2001; Philip *et al.*, 2012).

Discussion

We analysed the palaeohydrology within the framework of the evolutionary trajectory of the Markanda River valley. Evolutionary stages of the Markanda valley and its chronology were used to define palaeochannel geometry and to estimate palaeodischarge during the Late Holocene. The palaeodischarge values were compared with the SWAT model (and observation) based modern-day discharge to assess the changes in the river hydrology. Finally, we discuss the implications of large-scale hydrological changes in the foothill rivers from a high-discharge river to a reduced ephemeral river.

Morphological evolution of the Markanda valley

The UMV lies further west of the Kiarda Dun (Philip *et al.*, 2009), forming the westernmost extent of the Dehradun valley (Fig. 1). A comparison of morphological evolution of the Markanda valley with that of the Pinjaur, Kiarda Dun and Dehradun (Fig. 1) along with changes in the strength of the Indian Summer Monsoon is

presented in Figs. 8 and 9. In the Markanda valley, fan accretion, with characteristic sediments of proximal and distal fan setting (57.7 ± 1.9 ka) occurred during the Late Pleistocene. This aggradation might have continued similar to the filling of the accommodation space in the Pinjaur Dun and Dehradun (Fig. 8C) (Suresh *et al.*, 2007; Densmore et al., 2016; Sinha and Sinha, 2016). Besides the fan aggradation, development of fluvial terraces (T–1 and T–2) occurred in the Markanda valley. We do not have an age from the top of the distal fan in the Markanda valley; therefore, it is inferred that the fan sedimentation in the UMV ceased around 20 ka during the Last Glacial Maximum (LGM) corresponding to fan deposition (23.6 and 20.2 ka) in the Kiarda Dun (Philip *et al.*, 2009).

During the post-LGM, the Markanda valley witnessed valley incision corresponding to the incision in the Pinjaur Dun (Fig. 8B) (Suresh *et al.*, 2007) followed by aggradation of fluvial deposits (~13.1 ka) as observed in the T–3 terraces (Fig. 6C; Kala Amb section) during the terminal Pleistocene (Figs. 8 and 9). Rajaguru and Badam (1999) assigned a Late Pleistocene age to the T–3 terraces based on the presence of early Middle Palaeolithic artefacts (Joshi *et al.*, 1975). The post-LGM incision was initiated due to an increase in humidity and higher water volume in the river channel. It might have led to an increase in stream power and lowering of sediment concentration, which finally drive the incision process. As the climate changed with increased monsoonal strength during the Bølling–Allerød (15 to 12.9 ka; Dutt *et al.*, 2015), increased erosion and sediment supply provided sediment for deposition of the T–3 terrace during the early MIS-1 (Fig. 9C). The Early Holocene in the Markanda valley is recognised by the fluvial aggradation of T–4 and T–5 terraces along the Markanda River. The depositional age of the terrace sediment, ranging between 10.9 and 6.1 ka in the LMV, and 7.8 and 8.8 ka in the UMV, corresponds to the peak in the monsoon strength between 9 and 5 ka, the global Holocene climate optimum (Misra *et al.*, 2019).

Further, based on the geomorphic and sedimentary results, we infer that during the Late Holocene, the fine sediment of relatively young ages of ~3.8 ka near Kaunthra and ~3.9 ka near Kala Amb was deposited over the older T–3 fluvial terraces of early MIS-1 age (Fig. 6C–D). These younger sediments are recognised as palaeoflood deposits, suggesting extreme hydrological events in the Markanda valley during the

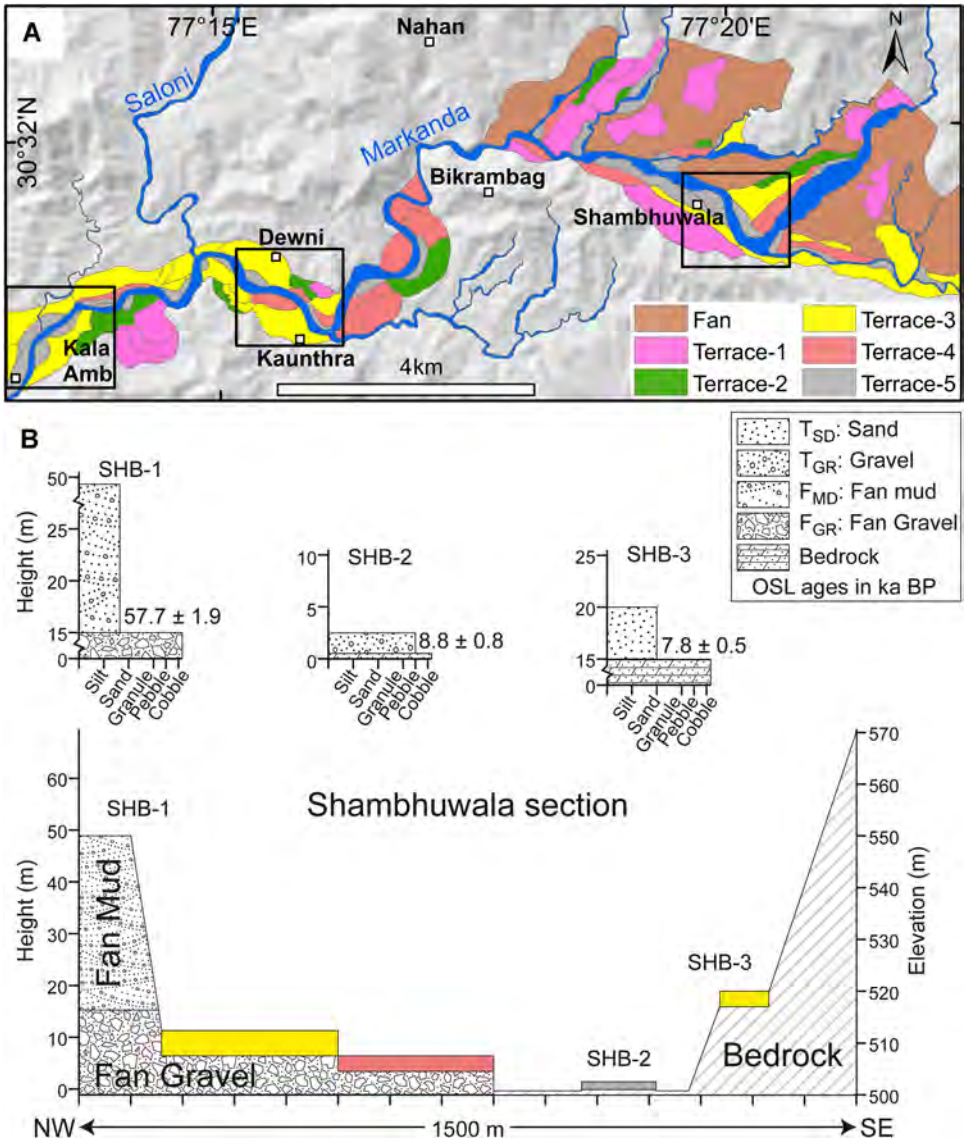

FIGURE 6 (A) Geomorphic map of the Markanda valley with boxes showing the study windows. Cross-section profiles of geomorphic units, and their vertical lithologs and depositional ages in the study windows. (B) Shambhuwala in UMV, (C) Kaunthra in the LMV, and (D) Kala Amb near the mountain front in the LMV. [Color figure can be viewed at wileyonlinelibrary.com]

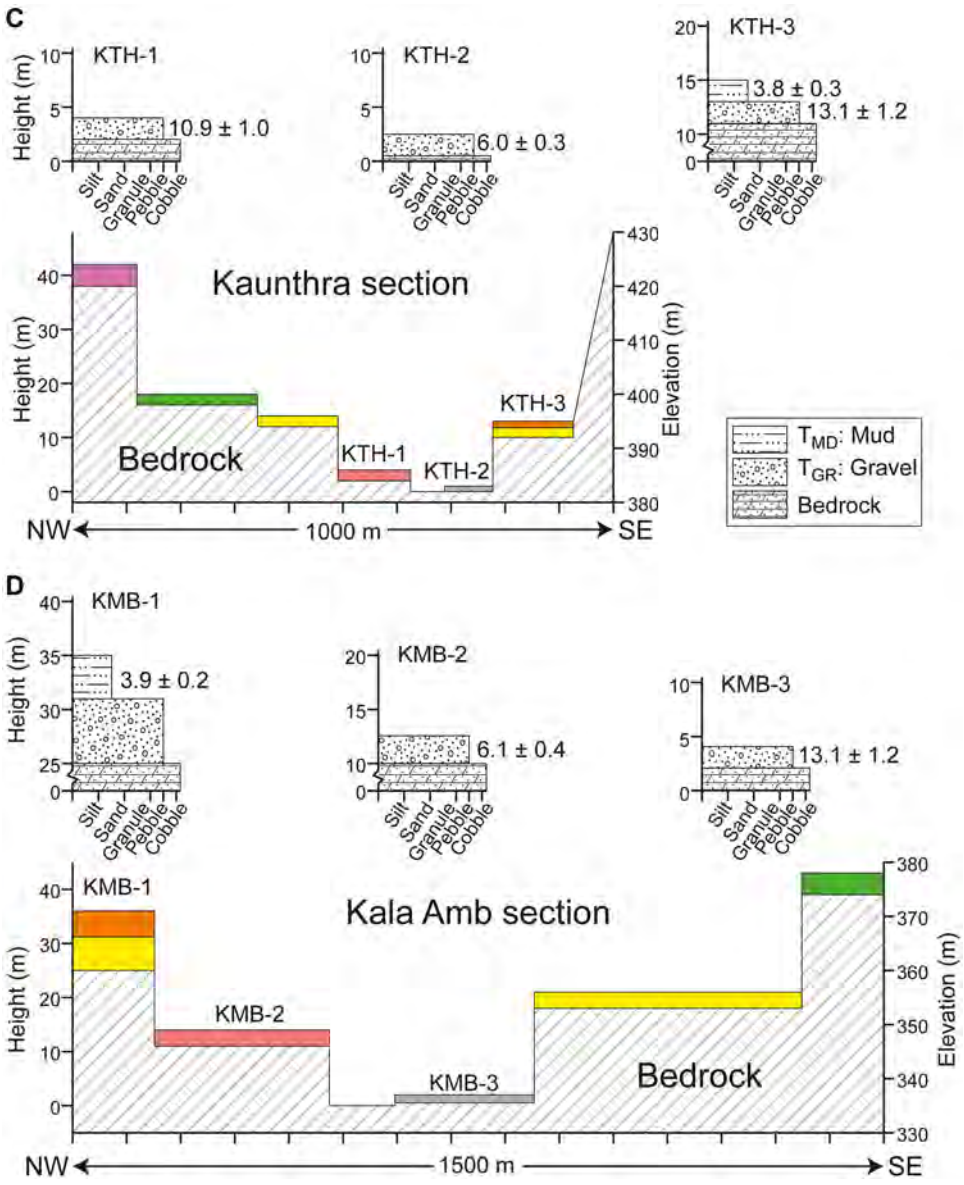

FIGURE 6 Continued

Late Holocene. Similar fine sediment cover on the fluvial terraces near the present study area was earlier reported by Rajaguru and Badam (1999), Kumar *et al.* (2001) and Philip *et al.*, (2012). Furthermore, similar terrace sequences with fine sediment cover on gravel sediment of strath terraces are documented in the nearby areas including Dehradun (Nakata, 1972; Fig. 3 of Wesnousky *et al.*, 1999; Singh *et al.*, 2001), and in the Yamuna valley (Dutta *et al.*, 2012).

We have used the records of Holocene climatic and tectonic events and assessed their impact by estimating aggradation and incision rates in the Markanda valley to infer the hydraulic geometry of the Markanda River during the deposition of palaeoflood sediment (at 3.9 ka) and to estimate palaeohydrological changes and their implication, as discussed in the following sections.

Palaeoflood discharge of foothill rivers

We used the palaeoflood deposits to estimate peak discharge of the Markanda River. The key uncertain component here is the channel cross-section geometry during the time of palaeoflood deposition. We used the modern-day cross-section and modified its depth using two different approaches at both upstream and downstream stations by considering (a) uplift rate across the channel and (b) channel processes. In the first approach, the amount of incision after the palaeoflood deposition was calculated by using a Late Holocene uplift rate of 4.8 ± 0.9 mm/year along the HFT near Kala Amb (Kumar *et al.*, 2001). This provides a total amount of incision in the range of 18.7 ± 3.6 m during the last 3.9 ± 0.2 ka. Adding this amount to the modern riverbed elevation (336 masl) suggests that the riverbed elevation at Kala Amb was 354.7 ± 3.6 masl at 3.9 ± 0.2 ka. The upstream Kaunthra site is far (~7 km) upstream of the HFT. Hence the impact of Late Holocene tectonics on the cross-section at Kaunthra was ignored and modern-day channel geometry was used to estimate palaeodischarge at Kaunthra.

In the second approach, palaeochannel hydraulic reconstruction was independently carried out through channel aggradation–degradation processes during the Holocene. For this, changes in riverbed levels were plotted using depositional ages and elevation of fluvial deposits at Kaunthra and Kala Amb (Fig. 10A). The riverbed elevation at Kaunthra was higher (394 masl) at 13.1 ± 1.2 ka as compared to the elevation (385 masl) at 6.0 ± 0.3 ka, suggesting riverbed incision at a rate of 1.3 ± 0.2 mm/

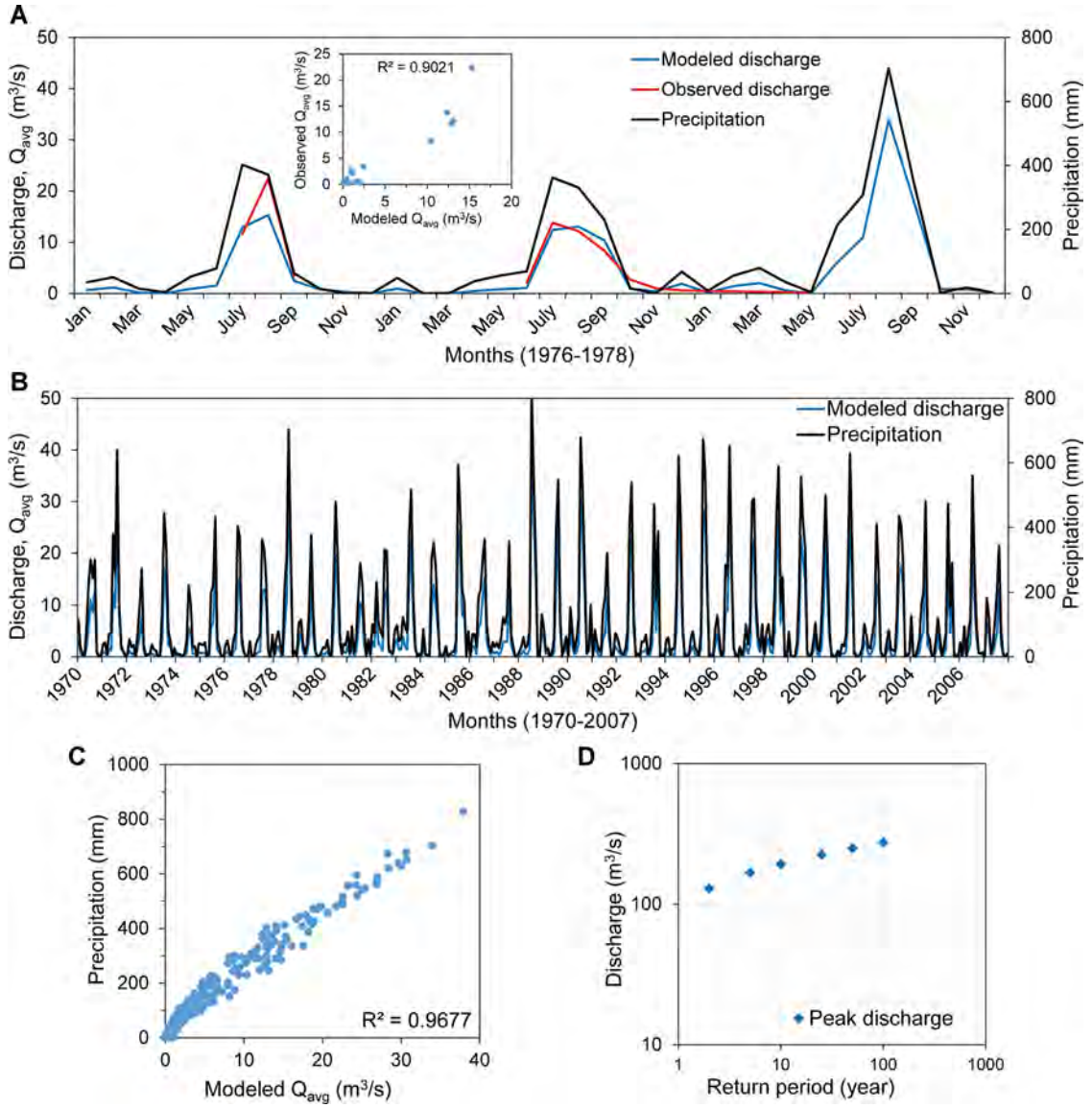

Figure 7. Observed and modelled discharge of the Markanda River. (A) comparison of SWAT modelled and observed mean monthly discharge along with the mean monthly precipitation data. Inset shows good correlation (R2=0.9) between observed and modelled mean monthly discharge. (B) SWAT modelled estimates of mean monthly discharge shown along the mean monthly precipitation data for the duration of 38 years (1970-2007). (C) a good correlation (R2=0.96) is observed between modelled estimates of mean monthly discharge and the mean monthly precipitation data. (D) Estimates of peak discharge using the log Pearson's type-III method for a different magnitude of flood events ranging from 2 to 200-year return period using SWAT modelled modern-day discharge data (1970-2007). Note the log-log axes in the plot. [Color figure can be viewed at wileyonlinelibrary.com]

year (Fig. 10B). Assuming this as the average incision rate, the riverbed at Kaunthra must have been incised to 382.2 ± 0.7 masl by 3.8 ± 0.3 ka, which is approximately the modern-day riverbed (382 masl). Therefore, the modern-day cross-section was used for the calculation of peak discharge at Kaunthra during palaeofloods (Fig. 11A). At the Kala Amb section the riverbed level was at a lower elevation (340 masl) at 13.1 ± 1.2 ka than the elevation (350 masl) at 6.1 ± 0.4 ka, suggesting riverbed aggradation at a rate of 1.4 ± 0.3 mm/year. Assuming this as the average aggradation rate, the riverbed at Kala Amb must have aggraded to 353.1 ± 0.8 masl at 3.9 ± 0.2 ka (Fig. 10B), nearly the same as the estimate (of 354.7 ± 3.6 masl) from our first approach and about 13 m below the elevation (366 masl) of the palaeoflood deposit. Therefore, 13 m of depth was used for the calculation of peak discharge in the modern-day cross-section of the Markanda River at Kala Amb (Fig. 11B).

Our estimates of peak discharge using different empirical equations show a wide range of values (Table S1). For further discussion, we preferred to use the values based on Manning's equation. The peak discharge at Kaunthra ($4.6 \times 10^3 \pm 0.4 \times 10^3$ m^3/s) and Kala Amb ($3.6 \times 10^4 \pm 0.6 \times 10^4$ m^3/s) during 3.8–3.9 ka (Fig. 11) indicates a significantly higher peak discharge, in comparison with modern peak discharge as well as 100-year return period discharge. The palaeochannel geometry at the upstream site is well constrained, as the channel cross-section at this site is very well controlled by known terrace surfaces (Fig. 11A), and no major changes have occurred in channel processes after 3.9 ka (Fig. 10B). Whereas, the channel downstream at Kala Amb is characterised by erosion processes after 3.9 ka (Fig. 10B), which might have enlarged the cross-section along the left bank. Excluding this enlarged cross-section, the peak discharge is estimated to be $3.3 \times 10^4 \pm 0.6 \times 10^4$ m^3/s at Kala Amb. Hence, we suspect that the enlarged cross-section because of left bank erosion at the downstream site might have led to an overestimated value of palaeodischarge. The higher value of peak discharges at Kala Amb with respect to Kaunthra may be partly due to a

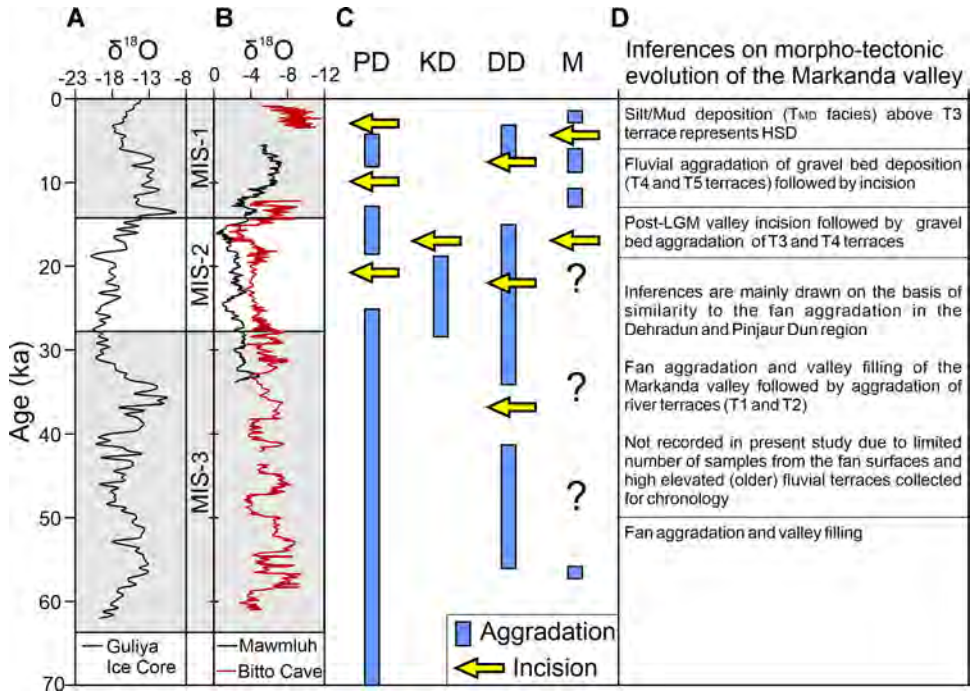

Figure 8. (A) A proxy record for past atmospheric temperature that drives regional scale monsoon circulations based on δ18O ice core record from the Guliya ice cap, Qinghai–Tibetan Plateau (Thompson et al., 1997) (B) terrestrial record of Indian monsoon variability based on high-resolution speleothem oxygen isotope (δ18O) record from Mawmluh cave (Dutt et al., 2015) and Bittoo cave (Kathayat et al., 2016). (C) Comparison of major aggradational and incisional event in the major intermontane valleys of NW Himalaya. PP- Pinjaur dun (Suresh et al., 2007), Kiarda Dun (Philip et al., 2009), DD-Dehradun (Densmore et al., 2016; Sinha and Sinha, 2016), M-Markanda valley (Present study). (D) interpretations on sedimentary environment and landform setting in the Markanda valley. [Color figure can be viewed at wileyonlinelibrary.com]

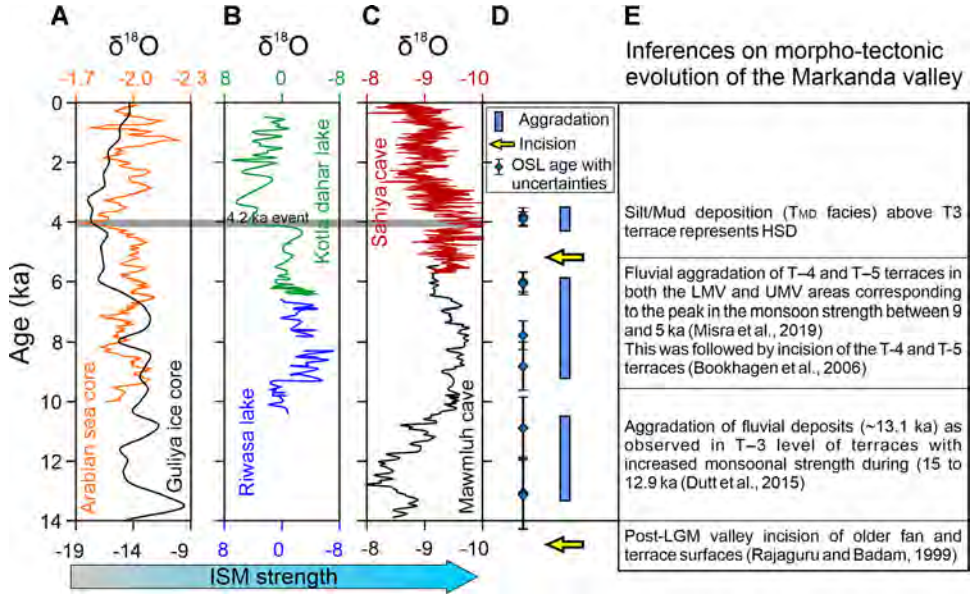

Figure 9. Changes in the strength of Holocene Indian Summer Monsoon (ISM). (A) δ18O of planktonic foraminifera off the Indus delta showing changes with a multi-centennial pacing (Staubwasser et al., 2003) and δ18O in the ice core from the Guliya ice cap, Qinghai–Tibetan Plateau (Thompson et al., 1997). (B) δ18O of gastropods from sediment in the lakes Riwasa (Dixit et al., 2014a) and Kotla Dahar (Dixit et al., 2014b). (C) high resolution records of δ18O in speleothems from caves Sahiya (Kathayat et al., 2018) and Mawmluh (Dutt et al., 2015). (D) OSL ages (with uncertainties) of the geomorphic units and inferred aggradation phases and incision event in the Markanda valley. (E) interpretations on evolution of fluvial landforms in the Markanda valley during the Holocene. [Color figure can be viewed at wileyonlinelibrary.com]

significant (57%) increase in the upstream basin area from 98.6 km^2 to 155 km^2, as Saloni River, along with other smaller tributaries, joins downstream of Kaunthra. Hence, we suggest that ≈ 4.6 × 10^3 m^3/s represents a minimum estimated value of palaeodischarge at 3.9 ka. This palaeodischarge value is several orders of magnitude higher than the modern average monthly discharge (22 m^3/s), peak summer discharge (245 m^3/s during 1990–2007) and the 100-year return period peak discharge (≈300 m^3/s) for the present-day Markanda River (Fig. 7D).

An alternate explanation for the Himalayan palaeoflood deposits is formation and breaches of landslides termed as landslide lake outburst floods (LLOF), often associated with phases strong monsoon/strong monsoon (Bookhagen *et al.*, 2005b; Gupta and Sah, 2008; Wasson *et al.*, 2008; Ruiz-Villanueva, *et al.*, 2017). However, such LLOF are

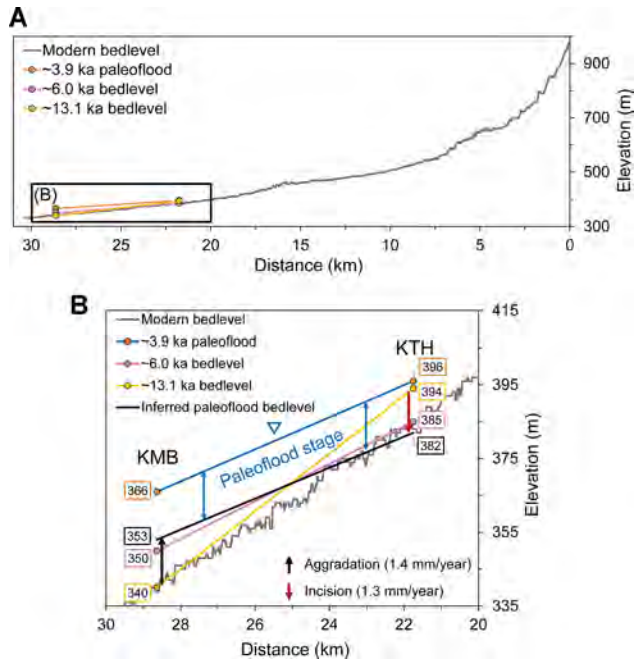

Figure 10. (A) Long profile of the Markanda River and isochron lines showing bedlevel at ~13.1 ka and ~6.0 ka, and paleoflood stage at ~3.9 ka between Kaunthra and Kala Amb sections. (B) bedlevel at ~13.1 ka is at higher and at ~6.0 ka is a lower elevation at upstream Kaunthra (KTH) section suggesting incision at a rate of 1.3 mm/year whereas at downstream Kala Amb (KMB) station, bedlevel at ~13.1 ka is at lower and at ~6.0 ka is at higher elevation suggesting aggradation at the rate of 1.4 mm/year. A paleoflood bedlevel is inferred by extending the incision and aggradation rates until ~3.9 ka at the Kaunthra and Kala Amb sections respectively. The paleoflood stage represented by ~3.9 ka isochron is based on flood deposits and is about 14 m and 13 m above the inferred paleoflood bedlevel at Kaunthra and Kala Amb sections respectively. Post 3.9 ka, the channel bed incised to modern day river bed level at downstream station. [Color figure can be viewed at wileyonlinelibrary.com]

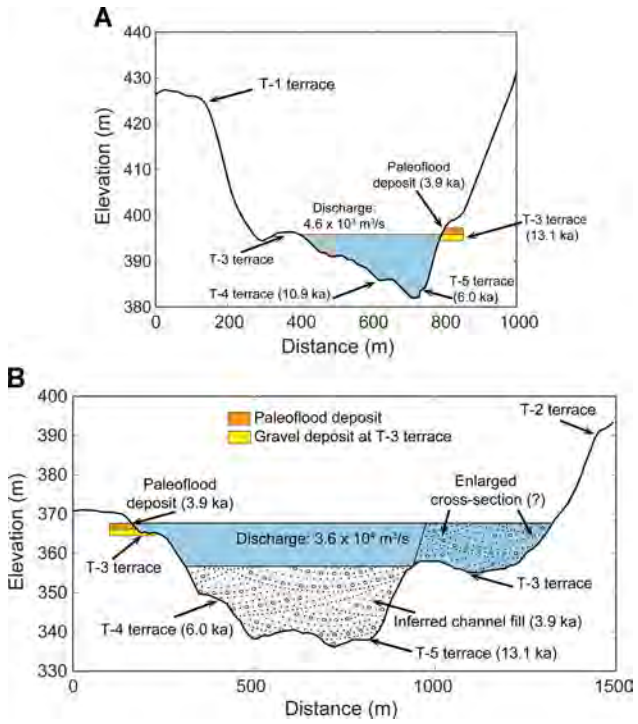

Figure 11. (A) River cross-section at Kaunthra showing estimated paleoflood peak discharge on the basis of location of paleoflood deposit and presence of various surfaces at left bank and right bank. (B) River cross section at Kala Amb showing channel fill (at 3.9 ka BP) and estimated peak paleoflood discharge (3.6 × 104 m3/s) on the basis of location of paleoflood deposit. Note that excluding the enlarged cross-section, the peak discharge becomes 3.3 × 104 m3/s suggesting possibility of overestimation due to the erosion process at Kala Amb. [Color figure can be viewed at wileyonlinelibrary.com]

spatially confined to high-elevation (> 4500 m) sectors of the Himalaya with a deep and narrow valley, and steep hillslopes near the threshold angle for failure, conducive for mass wasting (Bookhagen *et al.*, 2005b). In contrast, the present study area is located in the sub-Himalayas, having a low elevation (up to 1000 m), relatively broad valley and modest relief. Therefore, geomorphic characteristics of the river basin do not support the occurrence of LLOF, and hence we discard the possibility of LLOF to explain these palaeoflood deposits.

The regional extent of the palaeoflood event in our study is evident through the presence of similar sediment deposits, i.e. silty to sandy silt or loamy sand deposits overlying gravelly deposits of fluvial terraces, along the HFT in the northwest Himalaya (Wesnousky *et al.*, 1999; Kumar *et al.*, 2001, 2006; Philip *et al.*, 2012). Since these studies were focused on palaeoseismic investigations, they did not focus much on such deposits, except for hinting that they are a result of flood-related events. In particular, such deposits are mapped in foothill rivers along the Mohand range in the south of Dehradun (~3.7 kyr BP; Fig. 3 of Wesnousky *et al.*, 1999), suggesting the vast regional extent of such fluvial activity of foothill rivers after the mid-Holocene.

The palaeoflood deposit in the Markanda valley is a thick and massive accumulation of uniform deposition similar to that of floodplain sediment built up by regular inundation by peak discharges. Geomorphologically, the palaeoflood deposits also show significant spatial extent forming a veneer above the gravelly deposits of the T–3 terrace surfaces (Fig. 3A). Moreover, these palaeoflood deposits (3.8 to 3.9 ka) have a distinct chronological break from the underlying, much older, fluvial deposits (13.1 ka) of gravelly sediments representing the distinct low energy conditions of an active floodplain associated with a river channel, though, these observations can be inferred to be indicative of a high-discharge fluvial regime for the foothill rivers of the northwest Himalaya during the Late Holocene. However, we caution testing of such inferences, on possibility of hydrological shift, through future studies generating high-resolution data on sedimentology and chronology of the palaeoflood deposits along the foothill rivers of the northwest Himalaya. Nevertheless, the results of the present study can be interpreted to represent the occurrence of larger flooding event(s) in the foothill rivers of the northwest Himalaya during the Late Holocene. And this has implications, as discussed in next section, for understanding the fluvial landform evolution and its interaction with the past civilisation.

Implications for the G–H palaeochannel and Harappan civilisation

In the case of the Harappan civilisation, human–landscape interaction has been investigated from several perspectives and the role of river hydrology widely speculated about. The Harappan or Indus civilisation flourished mostly on vast alluvial plains, those of the Indus and its tributaries and of the Ghaggar–Hakra; its two largest cities, Harappa and Mohenjo-Daro, are adjacent to large perennial Himalayan rivers, while important urban centres such as Rakhigarhi, Farmana, Bhirrana, Banawali, Kalibangan or Ganwariwala are located along the palaeochannels in the Ghaggar–Hakra basin. Initially, large flooding events were proposed as the cause of

the demise of the civilisation (Dales, 1965; Raikes, 1964; Raikes and Dales, 1977), a thesis later criticised for lack of evidence (Possehl, 1967). A recent study suggested that fluvial quiescence of large Himalayan rivers and seasonal floods along monsoonal rivers fostered intensive agriculture that sustained the Harappan civilisation (Giosan *et al.*, 2012). Settlement patterns in spatio-temporal growth and decline with respect to the modern and palaeochannel river network highlight complex spatial heterogeneity as well as resilience and adaptation to a changing environment (Singh *et al.*, 2010; Gangal *et al.*, 2010; Petrie *et al.*, 2017; Dave *et al.*, 2019). However, the mechanisms for such heterogeneity are considered pinned to climate and related factors such as soil, irrigation, domesticated crops, livestock and ecology.

The chronological record for the disorganisation of the river system, represented by the G–H palaeochannel network in the northwest Indo-Gangetic plains, ranges from > 45 ka for its Yamuna branch (Clift *et al.*, 2012; Dave *et al.*, 2019) to the Early Holocene for the Sutlej branch (Clift *et al.*, 2012; Giosan *et al.*, 2012; Singh *et al.*, 2017). In contrast, a few studies reported mid-Holocene or younger dates and inferred a disorganised (Saini *et al.*, 2009) or rejuvenated (Chatterjee *et al.*, 2019) fluvial regime. Our results present the first hydrological assessment for the Markanda River, a tributary to the G–H palaeochannel, and shows a peak discharge during the Late Holocene several orders of magnitude higher than the modern discharge. Further, we noticed that similar palaeoflood deposits are present along the foothill rivers of the northwest Himalaya. Thus, we posit that the Himalayan foothill rivers had a better hydrological regime, having more flood events around 3.9 ± 0.2 ka, to sustain sufficient flows downstream in the Ghaggar–Hakra plain of Punjab, Haryana and Rajasthan during the Mature Harappan civilisation.

The mechanism for the proposed shift in the hydrological regime remains unclear, but we envisage that climatically controlled changes in the morphology of watersheds of the Himalayan foothill rivers governed their hydrological characteristics during the Late Holocene. Widespread climatic anomalies have been shown for the time interval between 4.2 and 3.9 ka, commonly referred to as the "4.2 ka event", as a long-term onset of aridity (Staubwasser *et al.*, 2003; Berkelhammer *et al.*, 2012; Dixit *et al.*, 2014b). Similar suggestions of an overall weakening of the Indian summer monsoonal rainfall are also available through pollen-based records and drying of lakes in northwest India (Singh *et al.*, 1972, 1974, 1990). In contrast, the strengthening of the east Asian winter monsoon (6.5–3.0 ka BP) using dust accumulation rates is reported from Chinese loess (Kang *et al.*, 2020). Moreover, the high-resolution record based on variability in $\delta^{18}O$ values of cave speleothems in the northwest Himalaya highlights the existence of multi-decadal diversity of Indian summer monsoon strength during the 4.2 and 3.9 ka time period (Kathayat *et al.*, 2018). Hence, palaeoclimate records suggest that long-term dominant patterns (of aridity or humidity) are also characterised by decadal- to centennial-scale variability in monsoon strength. However, the studied palaeoflood record also supports the occurrence of major flood events in the phase known for longer term aridity.

Our study is based on fluvial archives which are *in situ* representative of timing and past hydrology of a river system. It therefore brings forth a discussion on the significance of decadal scale variability in monsoon strength in river hydrology and processes in the largely favoured climatic model of aridity at 4.2 ka. An initial survey south of the HFT (near Kala Amb) shows wide occurrence of stratified gravelly fluvial deposits exposed in cliff sections along the Markanda River (Fig. S3). These can be explored in future studies to investigate the hydro-geomorphic history at the transition zone from the Himalayan foothill region to the Indo-Gangetic plains. The continuity in the Harappan culture in the Ghaggar–Hakra basin up to c. 3.9 ka is also a clear indication of its dependence on the river system; after c. 3.9 ka a gradual northward and northeastward movement of settlements is clearly noticed, while the near absence of Late Harappan settlements in the middle and lower courses of the river system supports its probable drying up or shifting (Fig. S4). Human settlements reappear only during the Painted Grey Ware period towards the middle and end of the second millennium BCE, with many of those settlements located within the channels, thus providing further evidence of their desiccation.

Conclusions

Recent studies have identified Himalayan catchment sources, mainly Sutlej and Yamuna rivers, for the sediment buried beneath the G–H palaeochannel and suggested Early to Mid-Holocene timing for the large-scale drainage reorganisation in this northwestern part of the Indo-Gangetic plains. However, the hydrology of the G–H palaeochannel during the time of the Harappan civilisation has remained unclear. In order to understand the human–landscape interaction with respect to the hydrology of the G–H palaeochannel we focus on the Markanda catchment upstream of channel Y1, a hypothesised palaeochannel of the Yamuna River. We analysed the sediment characteristics and depositional chronology of the fluvial terraces and fan surfaces in the Markanda valley in northwest India, chiefly to assess palaeohydrological conditions during the Late Holocene. These are the main conclusions:

(1) The geomorphology of the Markanda valley shows fan deposits in the UMV and five levels of fluvial terraces in the LMV. Terrace deposits dominantly consist of gravelly matrix-supported deposits with occasional sand lenses.
(2) The Markanda valley evolved at the westernmost extremity of the Dehradun valley, with alluvial fan aggradation during most of the Late Quaternary period. While terrace deposition began about the Mid to Late Pleistocene, such terraces (T–1 and T–2) are now situated at a higher elevation. T–3 terraces formed during the terminal Pleistocene.
(3) Valley incision and formation of T–4 and T–5 terraces mark the Holocene period. During the late Late Holocene, deposition of fine sediment over the gravelly deposits of the T–3 terraces is identified in the Markanda valley. These deposits represent a period of larger flooding conditions in the Himalayan foothill river.
(4) The peak discharge estimates for the palaeoflood deposits are several orders of magnitude higher than the modern-day average monthly discharge, as well as the 100-year return period peak discharge of the Markanda River.
(5) We infer that larger flooding of the Himalayan foothill rivers possibly supplied sufficient flows in the G–H palaeochannel to sustain Harappan settlements even on the banks of a declining river during the Mid-Holocene. The findings are largely substantiated by the presence of numerous Harappan sites in the Sutlej–Ghaggar system; only after 3.9 ka, the settlements moved upstream.
(6) A finer understanding of the mechanism for the mapped palaeoflood deposits in the foothill rivers would require detailed mapping and better chronological constraint of such deposits from other major foothill rivers along the transition zone of the Himalayan foothill region and Indo-Gangetic plains. Palaeoclimatology for high-resolution

record of changes in the Holocene monsoonal precipitation would also be needed to better understand controls on the hydrogeomorphic evolution of the foothill rivers.

Study area

In northwest Himalaya, the sub-Himalayan foreland basin between the Himalayan frontal thrust (HFT) and the main boundary thrust consists of Kangra re-entrant, Nahan salient and Dehradun re-entrant (Fig. 1). The Markanda valley lies between the Nahan salient and the Dehradun re-entrant, northwest Himalaya (Fig. 2). The ephemeral Markanda River originates in the Dharidhar range at an elevation of 1500 m in Himachal Pradesh. The river is separated from the Yamuna catchment by the Markanda–Bata drainage divide. The sub-Himalayan course of the Markanda River is ~30 km long down to Kala Amb, where it exits the Himalayan mountain front. The total basin area of the Markanda River at Kala Amb is ~155 km^2, which includes the ~41.2 km^2 area of its major tributary, Saloni River. In the Indo-Gangetic plains, the Markanda River flows through late Quaternary alluvial deposits to meet its trunk river, Ghaggar, a few kilometres southeast of the town of Shatrana (Fig. 1).

Litho-tectonic setup and climatic history

The Markanda River flows through Tertiary sediments, divided into the Siwalik Group (mid-Miocene to Late Pleistocene) and Subathu and Dagshai formations (Palaeocene to Oligocene) (Mathur, 1980; Najman *et al.*, 1994), whereas, the Quaternary deposits occur as alluvial fans and fluvial terraces (Table 1). The southern boundary of the sub-Himalaya is marked by the HFT, which brings the Tertiary rocks (middle Siwalik sandstones) over the Quaternary alluvium in the piedmont zone. At Kala Amb, a transverse fault termed as Kala Amb (or Black Mango) fault has displaced the HFT by over 5 km. Palaeoseismological studies suggested activities on the HFT between 29.3 ka and 17 ka, and between 5.8 ka and 2 ka (Philip *et al.*, 2012). Another study showed evidence of two to four large surface rupture earthquakes since 260 CE (Kumar *et al.*, 2001).

The study area's climate ranges from sub-humid in the Himalayan region to sub-arid in the plains region. The frontal region of northwest Himalaya gets monsoon rainfall of ~1000 to 1600 mm during summer and ~100 mm during winter (Rajaguru and Badam, 1999; Bookhagen *et al.*, 2005a). In the semi-arid plain, the average annual rainfall is 530 mm and the maximum rainfall is recorded during June to September. The discharge of the river is highly variable (58.2×10^6 m^3 in August to 0.5×10^6 m^3 in May) as observed for the period June 1976 to May 1978 at Kala Amb station (Parkash *et al.*, 1983). During the Quaternary, southwestern monsoons were weak during glacial maxima and strong during the early Holocene (Dhir *et al.*, 1994; Andrews *et al.*, 1998; Staubwasser *et al.*, 2003; Fleitmann *et al.*, 2003; Gupta *et al.*, 2003). During cold periods winter rains were relatively stronger in northwest India (Singh *et al.*, 1974; Wünnemann *et al.*, 2010; Giosan *et al.*, 2018). Intensified monsoon phases penetrated deep into the Sutlej valley during the Late Pleistocene (29–24 ka) and Holocene (10–4 ka) in the northwestern Himalaya (Bookhagen *et al.*, 2005b). The high-resolution speleothem oxygen isotope ($\delta^{18}O$) data from Bitto cave, shows millennial–orbital-scale variations in the Asian monsoon (Kathayat *et al.*, 2016). A synthesis of Indian subcontinent lake records shows a peak in monsoon strength (9 and 5 ka) corresponding to the global Holocene climate optimum (Misra *et al.*, 2019).

Archaeological context of the area

Human presence in the northwest Himalayas is evidenced from Acheulian sites of the Lower Pleistocene (700 to 400 ka) in the Siwalik ranges to Neolithic (3–1.5 ka) sites in the Kashmir Himalayas (Misra, 1987, Pappu, 2001; Gaillard *et al.*, 2010; Chauhan, 2010; Betts *et al.*, 2019). In particular, near Saketi village on a river terrace, Lower and Middle Palaeolithic tools have been found in the Markanda valley (Joshi *et al.*, 1975). The tools are made up of pebbles of quartzite and consist of uniaxial and bifacial choppers and scrapers (Rajaguru and Badam, 1999). Similarly, Acheulian to Neolithic collections of artefacts have been reported from terraces of the river Ghaggar in Pinjaur town in Pinjore–Nalagarh Dun (Mohapatra and Singh, 1979; Mohapatra, 1981; Karir *et al.*, 1983).

The Markanda valley lies upstream of channel Y1 and the G–H palaeochannel along which is the largest concentration of Harappan settlements (Dikshit, 1977, 1979; Joshi *et al.*, 1984; Gupta, 1996; Lal, 1997; Chakrabarti and Saini, 2009). The spatio-temporal patterns of these urban settlements are believed to be linked with rivers flowing in those palaeochannels (Agrawal, 1964; Wilhelmy, 1969; Misra, 1984, 2001; Courty, 1995; Agrawal and Pande, 1977; Pande, 1977; Kenoyer, 1998; Sahai, 1991; Madella and Fuller, 2006). The plains watered by the Ghaggar (Sarasvati) and Sutlej rivers were inhabited from at least the fourth millennium BCE, or as early as the sixth or seventh millennium BCE (Sarkar et al. 2016). To understand the linkage between rivers and civilisations, the initial analysis should be of palaeochannels' hydrology as an assessment of flow conditions during the Harappan period.

Acknowledgements. We duly acknowledge the financial support to this project granted by Research & Development, IIT Gandhinagar. We thank Taru Shikha Singh (Project Associate), Naman Jain (B Tech., 2019), and Akashsingh Rajput (PGDIIT, 2018 batch) IIT Gandhinagar for their help during topographical field surveys and sample collection. AS also thanks Dr Navin Juyal and Vinayak Kumar, PRL Ahmedabad for help and support during OSL dating. AS acknowledges discussions with Dr Ramendra Sahoo at various stages of the manuscript preparation. Finally, we thank two anonymous reviewers and Prof. Neil Roberts (Editor-in-chief) for their thoughtful and thorough reviews that improved the clarity of the manuscript.

Data availability statement

The data that support the findings of this study are available in the supplementary material for this article.

Supporting information

Additional supporting information can be found in the online version of this article.

Figure S1 Field photographs showing major geomorphic units. (A) In the upper Markanda valley, older fan deposits are cut across by the Markanda river. (B) in the lower Markanda valley fluvial strath terraces near the Kaunthra village. (C) and (D) respectively represents fluvial terraces on right and left banks of the Markanda river near the Kala Amb town close to Himalayan frontal thrust. Figure S2 Radial plots showing dose (Gray) distribution and overdispersion for all the samples. Note that sample mkd-8 is already shown in the figure 7 of the main text. Figure S3 (A) Google Earth satellite image of the

Markanda River basin shows different geomorphic features and locations of the field photographs. Yellow shaded area at bottom left marks the wide expanse of fluvial deposits of the Markanda River. (B) Field photographs shows the Markanda River south of the HFT. Panoramic view of the Markanda river shows incised reach from mountain exit in the upstream to ~1 km downstream. (C-D) Markanda River cliff-section shows stratified gravelly fluvial deposits suggesting continued bed-load transportation south of mountain exit. These deposits are incised relatively more than the terraces (T-4) mapped in the Kala Amb study window. These deposits can be further explored in future to understand hydro-geomorphic evolution of the Himalayan foothill region in response to the tectono-climatic changes. Figure S4 Site locations of different phases of the Harappan settlements (Possehl et al., 1999) around the G-H paleochannel in north-western India and Pakistan. (A) Mature (or Urban phase (2600-1900 BCE). (B) Late Harappan phase (1900-1300 BCE). (C) post-Harappan phase known as painted grey ware (1300-300 BCE). Note the desertion of the central and lower Ghaggar basin during late Harappan time. Table S1 Paleodischarge estimates using the Manning equation and constitutive flow resistance equations (based on the Manning and Chezy equations; Bjerklie et al., 2005).

References

Agrawal DP. 1964. Harappa culture: new evidence for a shorter chronology. *Science* **143**: 950–951.

Agrawal DP, Pande BM. 1977. *Ecology and Archaeology in Western India*. Concept Publishing Company: Delhi.

Andrews JE, Singhvi AK, Kailath AJ *et al*. 1998. Do stable isotopedata from calcrete record Late Pleistocene monsoonal climate variation in the Thar Desert of India. *Quaternary Research* **50**: 240–251.

Arnold JG, Srinivasan R, Muttiah RS *et al*. 1998. Large area hydrologic modeling and assessment part I: model development. *Journal of the American Water Resources Association (JAWRA)* **34**: 73–89.

Arnold LJ, Bailey RM, Tucker GE. 2007. Statistical treatment of fluvial dose distributions from southern Colorado arroyo deposits. *Quaternary Geochronology* **2**: 162–167.

Baker VR. 1973. Paleohydrology and sedimentology of Lake Missoula flooding in eastern Washington (Vol. 144). Geological Society of America.

Baker VR, Kochel RC, Patton PC *et al*. 1983. Palaeohydrologic analysis of Holocene flood slack-water sediments. In *Modern and ancient fluvial systems* Collinson JD, Lewin J (eds). Wiley; 229–239.

Baker VR. 1987. Paleoflood hydrology and extraordinary flood events. *Journal of Hydrology* **96**: 79–99.

Baker VR. 2008. Paleoflood hydrology: Origin, progress, prospects. *Geomorphology* **101**(1-2): 1–13.

Bauer T, Klinger RE. 2010. *Evaluation of paleoflood peak discharge estimates in hydrologic hazard studies*. Report DSO–11–03. Dam Safety Technology Development Program. U.S. Department of the Interior Bureau of Reclamation Technical Service Center Geotechnical Services Division Seismotectonics and Geophysics Group Denver, Colorado.

Berkelhammer M, Sinha A, Stott L *et al*. 2012. An abrupt shift in the Indian monsoon 4000 years ago. *Geophysical Monograph Series* **198**: 75–87.

Betts A, Yatoo M, Spate M *et al*. 2019. The Northern Neolithic of the Western Himalayas: New Research in the Kashmir Valley. *Archaeological Research in Asia* **18**: 17–39.

Bjerklie DM, Dingman SL, Bolster CH. 2005. Comparison of constitutive flow resistance equations based on the Manning and Chezy equations applied to natural rivers. *Water Resources Research* **41**(11): W11502.

Bookhagen B, Thiede RC, Strecker MR. 2005a. Abnormal monsoon years and their control on erosion and sediment flux in the high, arid northwest Himalaya. *Earth and Planetary Science Letters* **231**(1–2): 131–146.

Bookhagen B, Thiede RC, Strecker MR. 2005b. Late Quaternary intensified monsoon phases control landscape evolution in the northwest Himalaya. *Geology* **33**(2): 149–152.

Chakrabarti DK, Saini S. 2009. *The Problem of the Saravati River and Notes on the Archaeological Geography of Haryana and Indian Punjab*. Aryan Books: Delhi.

Chatterjee A, Ray JS, Shukla AD *et al*. 2019. On the existence of a perennial river in the Harappan heartland. *Scientific Reports* **9**(1): 1–7.

Clift PD, Carter A, Giosan L *et al*. 2012. U-Pb zircon dating evidence for a Pleistocene Sarasvati River and capture of the Yamuna River. *Geology* **40**(3): 211–214.

Chauhan PR. 2010. Comment on 'Lower and Early Middle Pleistocene Acheulian in the Indian sub-continent'by Gaillard *et al*. (2009) (Quaternary International). *Quaternary International* **223**: 248–259.

Chauhan N, Singhvi AK. 2011. Distribution in sar palaeodoses due to spatial heterogeniety of natural beta dose. *Geochronometria* **38**: 190–198.

Chauhan N, Morthekai P. 2017. Chronology of desert margin in western India using improved luminescence dating protocols. *Journal of Earth System Science* **126**(8): 115.

Courty M-A. 1995. Late Quaternary environmental changes and natural constraints to ancient land use (Northwest India). In *Ancient People and Landscapes*, Johnson E (ed). Museum of Texas Technical University: Lubbock; 106–126.

Dales GF. 1965. Civilisation and floods in the Indus Valley. *Expedition* **7**(4): 10.

Danino M. 2010. *The lost river: On the trail of the Sarasvatī*. Penguin Books: India.

Dave AK, Courty MA, Fitzsimmons KE *et al*. 2019. Revisiting the contemporaneity of a mighty river and the Harappans: Archaeological, stratigraphic and chronometric constraints. *Quaternary Geochronology* **49**: 230–235.

Densmore AL, Sinha R, Sinha S *et al*. 2016. Sediment storage and release from Himalayan piggyback basins and implications for downstream river morphology and evolution. *Basin Research* **28**(4): 446–461.

Dikshit KN. 1977. Distibution and relationship of protohistoric sites along old river channels of the Ghaggar system. In *Ecology and Archaeology in Western India*, Agrawal DP, Pande BM (eds). Concept Publishing Company: Delhi; 61–66.

Dixit Y, Hodell DA, Sinha R. *et al*. 2014a. Abrupt weakening of the Indian summer monsoon at 8.2 kyr B.P. *Earth and Planetary Science Letters*. **391** 16–23.

Dixit Y, Hodell DA, Petrie CA. 2014b. Abrupt weakening of the summer monsoon in northwest India~ 4100 yr ago. *Geology* **42**(4): 339–342.

Dikshit KN. 1979. Old channels of Ghaggar in Rajasthan-revisited. *Man and Environment* **3**: 105–106.

Dhir RP, Rajaguru SN, Singhvi AK. 1994. Desert Quaternary formations and their morphostratigraphy: implications for Quaternary history of the Thar Desert. *Journal of the Geological Society of India* **43**(4): 435–447.

Durcan JA, Thomas DS, Gupta S *et al*. 2019. Holocene landscape dynamics in the Ghaggar-Hakra palaeochannel region at the northern edge of the Thar Desert, northwest India. *Quaternary International* **501**: 317–327.

Dutt S, Gupta AK, Clemens SC *et al*. 2015. Abrupt changes in Indian summer monsoon strength during 33,800 to 5500years B.P. *Geophysical Research Letters* **42**: 5526–5532.

Dutta S, Suresh N, Kumar R. 2012. Climatically controlled Late Quaternary terrace staircase development in the fold-and-thrust belt of the Sub Himalaya. *Palaeogeography, Palaeoclimatology, Palaeoecology* **356**: 16–26.

Farr TG, Rosen PA, Caro E *et al*. 2007. The shuttle radar topography mission. *Reviews of Geophysics* **45**(2): RG2004.

Fleitmann D, Burns SJ, Mudelsee M *et al*. 2003. Holocene forcing of the Indian monsoon recorded in a stalagmite from southern Oman. *Science* **300**: 1737–1739.

Gaillard C, Mishra S, Singh M *et al*. 2010. Lower and Early Middle Pleistocene Acheulian in the Indian sub-Continent. *Quaternary International* **223–224**: 234–241.

Gangal K, Vahia MN, Adhikari R. 2010. Spatio-temporal analysis of the Indus urbanization. *Current Science* 846–852.

Giosan L, Clift PD, Macklin MG *et al*. 2012. Fluvial landscapes of the Harappan civilization. *Proceedings of the National Academy of Science of the USA* **109**(26) E1688–E1694.

Giosan L, Orsi WD, Coolen M *et al*. 2018. Neoglacial climate anomalies and the Harappan metamorphosis. *Climate of the Past* **14**: 1669–1686.

Guha S, Singh A, Kaushal RK. 2020. ChanGe: A MATLAB based tool for calculation of channel hydrological parameters. *Current Science* **119**: 741–742.

Gupta SP. 1996. *The Indus–Sarasvatí Civilization: Origins, Problems and Issues* Pratibha Prakashan: Delhi.

Gupta AK, Anderson DM, Overpeck JT. 2003. Abrupt changes in the Asian southwest monsoon during the Holocene and their links to the North Atlantic Ocean. *Nature* **421**: 354–356.

Gupta V, Sah MP. 2008. Impact of the trans-Himalayan landslide lake outburst flood (LLOF) in the Satluj catchment, Himachal Pradesh, India. *Natural Hazards* **45**(3): 379–390.

Haan CT. 1977. *Statistical methods in hydrology*. The Iowa State University Press

Joshi RV, Rajaguru SN, Pappu RS *et al*. 1974. Quaternary Glaciation and Palaeolithic sites in the Liddar Valley (J & K). *World Archaeology* **5**: 369–379.

Joshi RV, Rajaguru SN, Badam GL *et al*. 1975. Early and middle Palaeolithic tools from river terraces in the Saketi area, markanda valley, Himachal Pradesh. *Current Science* **44**(13): 464–465.

Joshi JP, Bala M, Ram J. 1984. The Indus Civilization: a reconsideration on the basis of distribution maps. In *Frontiers of the Indus Civilization*, Lal BB, Gupta SP (eds). Books and Books: New Delhi; 511–530.

Kale VS, Singhvi AK, Mishra PK *et al*. 2000. Sedimentary records and luminescence chronology of Late Holocene palaeofloods in the Luni River, Thar Desert, northwest India. *Catena* **40**: 337–358.

Kang S, Du J, Wang N *et al*. 2020. Early Holocene weakening and mid-to late Holocene strengthening of the East Asian winter monsoon. *Geology* **48**(11): 1043–1047.

Karir BS, Chopra SRK, Suneja IJ. 1983. Observation on stratigraphy of archaeologically significant river terraces in some parts of Pinjore-Nalagarh Dun (NW India). *Indian Anthropologist* **13**(1): 31–35.

Kaushal RK, Sarkar A, Mishra K *et al*. 2020. Spatio-temporal variability in stream power distribution in the Upper Kosi River basin, Central Himalaya: Controls and geomorphic implications. *Geomorphology* **350**: 106888.

Kathayat G, Cheng H, Sinha A *et al*. 2016. Indian monsoon variability on millennial-orbital timescales. *Scientific Reports* **6**: 24374.

Kathayat G, Cheng H, Sinha A *et al*. 2018. Evaluating the timing and structure of the 4.2 ka event in the Indian summer monsoon domain from an annually resolved speleothem record from Northeast India. *Climate of the Past* **14**(12): 1869–1879.

Kenoyer JM. 1998. *Ancient Cities of the Indus Valley Civilization*. Oxford University Press: Karachi.

Khan I, Sinha R. 2019. Discovering 'buried' channels of the Palaeo-Yamuna river in NW India using geophysical evidence: Implications for major drainage reorganization and linkage to the Harappan Civilisation. *Journal of Applied Geophysics* **167**: 128–139.

Kumar S, Wesnousky SG, Rockwell TK *et al*. 2001. Earthquake recurrence and rupture dynamics of Himalayan Frontal Thrust, India. *Science* **294**(5550): 2328–2331.

Kumar S, Wesnousky SG, Rockwell TK *et al*. 2006. Paleoseismic evidence of great surface rupture earthquakes along the Indian Himalaya. *Journal of Geophysical Research: Solid Earth* **111**(B3).

Lal BB. 1997. *The Earliest Civilisation of South Asia*. Aryan Books International: New Delhi.

Macklin G, Lewin J. 2015. The rivers of civilization. *Quaternary Science Reviews* **14**: 28—44.

Madella M, Fuller DQ. 2006. Paleoecology and the Harappan civilisation of South Asia: a reconsideration. *Quaternary Science Reviews* **25**: 1283–1301.

Mathur NS. 1980. Biostratigraphical aspects of the Subathu Formation, Kumaun Himalaya. *Recent Researches in Geology* **5**: 96–112.

Misra VN. 1984. Climate, a factor in the rise and fall of the Indus Civilization. In *Frontiers of the Indus Civilization*, Lal BB, Gupta SP (eds). Books and Books: New Delhi; 461–489.

Misra VN. 1987. Middle Pleistocene adaptations in India. In *The Pleistocene Old World: Regional Perspectives*, Soffer O (ed). Plenum Press: New York; 99–119.

Misra VN. 2001. The role of the ṛgvedic sarasvatī in the rise, growth and decline of the indus civilization. *Annals of the Bhandarkar Oriental Research Institute* **82**(1/4): 165–191.

Misra P, Tandon SK, Sinha R. 2019. Holocene climate records from lake sediments in India: Assessment of coherence across climate zones. *Earth-Science Reviews* **190**: 370–397.

Mohapatra GC, Singh M. 1979. Stratified occurrence of lithic artifacts in the Siwalik frontal range of western sub-Himalaya. *Punjab University Research Bulletin* **10**(1-2): 65–77.

Mohapatra GC. 1981. Acheulian discoveries in the Siwalik frontal range. *Current Anthropology* **22**(4): 433–435.

Murray AS, Wintle AG. 2000. Luminescence dating of quartz using an improved single–aliquot regenerative–dose protocol. *Radiation Measurements* **32**: 57–73.

Nakata T. 1972. Geomorphic history and crustal movements of foothills of the Himalayas. *Science Reports of the Tohuku, University, 7th Series: Geography* **22**(1): 177.

Najman YM, Enkin RJ, Johnson MR *et al*. 1994. Palaeomagnetic dating of the earliest continental Himalayan foredeep sediments: Implications for Himalayan evolution. *Earth and Planetary Science Letters* **128**(3–4): 713–718.

O'Connor JE. 1993. *Hydrology, hydraulics, and geomorphology of the Bonneville flood* (Vol. 274). Geological Society of America.

Oldham CF. 1874. Notes on the lost river of the Indian desert. *Calcutta Review* **49**: 1–29.

Oldham RD. 1886. On probable changes in the geography of the Punjab and its rivers: an historico-geographical study. *Journal of Asiatic Society of Bengal* **55**: 322–343.

Pal Y, Sahai B, Sood RK *et al*. 1980. Remote sensing of the 'lost' Saraswati' river. *Proceedings, Indian Academy of Sciences (Earth and Planetary Sciences)* **89**: 317–331.

Pande BM. 1977. Archaeological remains of the ancient Saraswati. In *Ecology and Archaeology in Western India*, Agrawal DP, Pande BM (eds). Concept Publishing Company: Delhi; 125–129.

Pappu RS. 2001. *Acheulian Culture in Peninsular India*. D.K. Printworld (P) Ltd: New Delhi.

Parkash B, Awasthi AK, Gohain K. 1983. Lithofacies of the Markanda terminal fan, Kurukshetra district, Haryana, India. In *Modern and ancient fluvial systems* International Association of Sedimentologists **6**: 337–344.

Petrie CA, Singh RN, Bates J *et al*. 2017. Adaptation to variable environments, resilience to climate change: Investigating land, water and settlement in Indus Northwest India. *Current Anthropology* **58**(1): 1–30.

Philip G, Virdi NS, Suresh N. 2009. Morphotectonic evolution of Parduni Basin: An intradun piggyback basin in western Doon valley, NW Outer Himalaya. *Journal of the Geological Society of India* **74**(2): 189–199.

Philip G, Bhakuni SS, Suresh N. 2012. Late Pleistocene and Holocene large magnitude earthquakes along Himalayan Frontal Thrust in the central seismic gap in NW Himalaya, Kala Amb, India. *Tectonophysics* **580**: 162–177.

Possehl GL. 1967. The Mohenjo-daro Floods: A Reply 1. *American anthropologist* **69**(1): 32–40.

Possehl GL. 1999. *Indus Age: The Beginnings*. University of Pennsylvania Museum: Philadelphia, PA.

Puri VMK. 1999. Vedic Sarasvati: Scientific signatures on its origin from the Himalaya. In *Vedic River Sarasvati Hindu Civilization*, Kalyanaraman S (ed). Aryan books international: New Delhi; 14–35.

Raiverman V, Kunte SV, Mukherjea A. 1983. Basin geometry, Cenozoic sedimentation and hydrocarbon prospects in northwestern Himalaya and Indo-Gangetic plains. *Petroleum Asia Journal* **6**(IV): 67–92.

Raikes RL. 1964. The end of the ancient cities of the Indus. *American Anthropologist* **66**(2): 284–299.

Raikes RL, Dales GF. 1977. The Mohenjo-daro floods reconsidered. *Journal of the Palaeontological Society of India* **20**: 251–260.

Rajaguru SN, Badam GL. 1999. Late Quaternary Geomporphology and Environment of the Markanda valley, Himachal Pradesh. *Memoir Geological Society of India* **42**: 143–151.

Rennel J. 1788. *Memoir of a Map of Hindoostan; or the Moghul Empire* London.

Ruiz-Villanueva V, Allen S, Arora M *et al*. 2017. Recent catastrophic landslide lake outburst floods in the Himalayan mountain range. *Progress in Physical Geography* **41**(1): 3–28.

Sahai B. 1991. Unraveling of the 'lost' vedic Saraswati, *Memoir, Geological Society of India* **42**: 121–141.

Saini H, Tandon S, Mujtaba S *et al*. 2009. Reconstruction of buried channel-floodplain systems of the northwestern Haryana Plains. *Current Science* **97**(11.

Sarkar A, Mukherjee AD, Bera MK *et al*. 2016. Oxygen isotope in archaeological bioapatites from India: Implications to climate change and decline of Bronze Age Harappan civilization. *Scientific Reports* **6**(1): 1–9.

Singh G, Joshi RD, Singh AB. 1972. Stratigraphic and radiocarbon evidence for the age and development of three salt lake deposits in Rajasthan, India. *Quaternary Research* **2**(4): 496–505.

Singh G, Joshi RD, Chopra SK *et al*. 1974. Late Quaternary history of vegetation and climate of the Rajasthan Desert, India. *Philosophical Transactions of the Royal Society of London. B, Biological Sciences* **267**(889): 467–501.

Singh G, Wasson RJ, Agrawal DP. 1990. Vegetational and seasonal climatic changes since the last full glacial in the Thar Desert, northwestern India. *Review of Palaeobotany and Palynology* **64**(1–4): 351–358.

Singh AK, Parkash B, Mohindra A *et al*. 2001. Quaternary alluvial fan sedimentation in the Dehradun Valley Piggyback Basin, NW Himalaya: tectonic and palaeoclimatic implications. *Basin Research* **13**: 449–471.

Singh RN, Petrie CA, Pawar V *et al*. 2010. Changing patterns of settlement in the rise and fall of Harappan urbanism and beyond: a preliminary report on the Rakhigarhi Hinterland Survey 2009. *Man and Environment* **35**(1): 37–53.

Singh A, Thomsen KJ, Sinha R *et al*. 2017. Counter-Intuitive influence of Himalayan river morphodynamics on Indus Civilisation urban settlements. *Nature Communications* **8**(1617): 1–14.

Singh A, Sinha R. 2019. Fluvial response to climate change inferred from sediment cores from the Ghaggar–Hakra paleochannel in NW Indo–Gangetic plains. *Palaeogeography, Palaeoclimatology, Palaeoecology* **532**: 109247.

Sinha S, Sinha R. 2016. Geomorphic evolution of Dehra Dun, NW Himalaya: Tectonics and climatic coupling. *Geomorphology* **266**: 20–32.

Srivastava P, Kumar A, Chaudhary S *et al*. 2017. Paleofloods records in Himalaya. *Geomorphology* **284**: 17–30.

Staubwasser M, Sirocko F, Grootes PM *et al*. 2003. Climate change at the 4.2 ka BP termination of the Indus valley civilization and Holocene south Asian monsoon variability. *Geophysical Research Letters* **30**: 1425.

Stein A. 1917. On Some River Names in the Ṛgveda. *The Journal of the Royal Asiatic Society of Great Britain and Ireland* 91–99.

Stein A. 1942. A survey of ancient sites along the 'lost' Saraswati river. *Geographical Journal* **99**: 173–182.

Suresh N, Bagati TN, Kumar R *et al*. 2007. Evolution of Quaternary alluvial fans and terraces in the intramontane Pinjaur Dun, Sub-Himalaya, NW India: interaction between tectonics and climate change. *Sedimentology* **54**(4): 809–833.

Thompson LG, Yao T, Davis ME *et al*. 1997. Tropical climate instability: the last Glacial cycle from a Qinghai–Tibetan ice core. *Science* **276**: 1821–1825.

Tod J, Lt-Col. 1832. *Annals and Antiquities of Rajasthan, London, 1829–32*; republ. Lolit Mohun Audhya: Calcutta, 1894.

Tsakalos E, Christodoulakis J, Charalambous L. 2016. The Dose Rate Calculator (DRc) for Luminescence and ESR Dating–a Java Application for Dose Rate and Age Determination. *Archaeometry* **58**: 347–352.

Valdiya KS. 2002. *Saraswati: the River That Disappeared*. Universities Press: Hyderabad.

Valdiya KS. 2017. *Prehistoric River Saraswati, Western India*. Society of earth scientists series. Springer International Publishing. 1–136.

Vivien de Saint-Martin L. 1860. *Étude sur la géographie et les populations primitives du nord-ouest de l'Inde, d'après les hymnes védiques* Imprimerie Impériale: Paris.

Wasson RJ, Juyal N, Jaiswal M, *et al*. 2008. The mountain-lowland debate: Deforestation and sediment transport in the upper Ganga catchment. *Journal of Environmental Management,* **88**(1):53–61.

Wasson RJ, Smith GI, Agrawal DP. 1984. Late Quaternary sediments, minerals, and inferred geochemical history of Didwana Lake, Thar Desert, India. *Palaeogeography, Palaeoclimatology, Palaeoecology* **46**(4): 345–372.

Wesnousky SG, Kumar S, Mohindra R *et al*. 1999. Uplift and convergence along the Himalayan Frontal Thrust. *Tectonics* **18**(6): 967–976.

Wilhelmy H. 1969. Das urstomtal zur Ostrand der Indisebene und das Sarasvatiproblem. *Zeitschrift fuer Geomorphologie. N.F., Suppl.* **8**: 76–93.

Wünnemann B, Demske D, Tarasov P *et al*. 2010. Hydrological evolution during the last 15 kyr in the Tso Kar lake basin (Ladakh, India), derived from geomorphological, sedimentological and palynological records. *Quaternary Science Reviews* **29**: 1138–1155.